Materials & Design 246 (2024) 113334

Contents lists available at ScienceDirect

Materials & Design

journal homepage: www.elsevier.com/locate/matdes

Robotic skins inspired by auxetic metamaterials for programmable bending of soft actuators

Yichen Pu [a], Shengwei Zheng [a], Xinjie Hu [a], Shan Tang [b], Ning An [a,b,*]

[a] Key Laboratory of Advanced Spatial Mechanism and Intelligent Spacecraft, Ministry of Education, School of Aeronautics and Astronautics, Sichuan University, Chengdu 610065, People's Republic of China

[b] State Key Laboratory of Structural Analysis for Industrial Equipment, Dalian University of Technology, Dalian 116023, People's Republic of China

ARTICLE INFO

Dataset link: https://github.com/SCU-An-Group/Metamaterial-Skins-for-Soft-Actuators

Keywords:
Robotic skins
Auxetic metamaterials
Pneumatic actuators
Programmable bending
Soft robotics

ABSTRACT

This paper presents a class of robotic skins inspired by auxetic metamaterials, which enable programmable bending in soft pneumatic actuators. The efficiency of these robotic skins in controlling bending curvature and hoop expansion of the soft actuators is demonstrated through a combination of experiments and numerical simulations. Parametric studies are then performed to explore how variations in the geometric parameters of the metamaterial skin affect the performance of the bending actuators. Specifically, our study demonstrates that a range of bending curvatures (0.0077 mm^{-1} to 0.0097 mm^{-1}) and cross-section diameters (38.4 mm to 44.0 mm) can be achieved by adjusting the unit cell numbers of metamaterial skin in the vertical and hoop directions for bending a 2 mm-thickness-walled inflatable cylindrical tube, which is characterized by an initial length of 104.3 mm, an initial cross-section diameter of 29.0 mm, and at an inflation volume of 75 mL. Moreover, a variety of bio-inspired soft actuators exhibiting complex bending behaviors are presented. The work demonstrates the effectiveness of the proposed strategy for achieving customized curved bending and shape-morphing by adjusting the geometric parameters and arrangement of the unit cells in the metamaterial skins.

1. Introduction

Soft robotics has emerged as a prominent topic in recent decades, attracting the interest of researchers, engineers, and innovators across diverse fields [1–3]. This field focuses on the design and creation of robots made from soft and flexible materials, diverging from traditional rigid robots. Bending serves as a fundamental deformation mode in the design of soft robots, playing a vital role in enabling their diverse functionality and versatility. The ability to achieve programmable bending is crucial as it allows soft robots to adapt to various tasks and environments with precision and efficiency. This capability finds applications across a broad spectrum of fields, including soft grippers for delicate object manipulation [4–6], morphing structures for shape-shifting capabilities [7,8], bio-inspired robotics for mimicking natural movements [9,10], and biomedical devices for surgery, diagnosis, drug delivery, and wearable and assistive devices [11]. In each of these examples, the continuous and smooth bending of soft materials enables robots to perform tasks that are challenging or impossible for traditional rigid robots, highlighting the significance of programmable bending in advancing the capabilities of soft robotic systems.

A fundamental type of soft robot utilizes pneumatic-powered actuators. These actuators are typically constructed from rubber-like flexible materials and consist of a series of chambers embedded inside. The chambers inflate like balloons upon pumping air to generate actuation [12]. Various methods have been proposed to achieve bending in such soft robots through pneumatic actuation. Some studies adopt asymmetrical material and geometry distributions of pneumatic chambers to induce bending motion upon pressurization. When one side of the chamber has thinner walls compared to the other side, it experiences greater expansion or elongation when pressurized [13–15]. This imbalance in expansion results in bending of the chamber to accommodate the differential elongation of the material. While the asymmetrical design facilitates bending in a desired direction, the chamber may also expand in other directions due to the pressure exerted by the inflating air. This multidirectional expansion can result in undesired motions or deformations, potentially reducing the efficiency or controllability of the bending of the soft robots and limiting the precision and accuracy

* Corresponding author at: Key Laboratory of Advanced Spatial Mechanism and Intelligent Spacecraft, Ministry of Education, School of Aeronautics and Astronautics, Sichuan University, Chengdu 610065, People's Republic of China.
E-mail address: anning@scu.edu.cn (N. An).

https://doi.org/10.1016/j.matdes.2024.113334
Received 27 May 2024; Received in revised form 17 September 2024; Accepted 24 September 2024
Available online 27 September 2024

of tasks that the robot can perform. To mitigate this issue, additional structural elements can be incorporated with the soft actuator to guide the bending deformation in a specific direction. Strain-limiting layers and pneumatic networks can be employed to restrict the expansion of the chamber in undesirable directions [16,17]. Additionally, fiber-reinforced materials [18–22], and knit fabrics [23–26] can be integrated into the soft actuator to enhance its stiffness and guide the bending deformation along specific pathways.

Mechanical metamaterials are artificially engineered materials that provide unique properties not found in natural materials [27–29]. Through rational design of microstructural geometry, they can achieve extreme and programmable properties, such as negative Poisson's ratio and on-demand stiffness [30,31]. Employing mechanical metamaterials as specialized robotic skins to reinforce the inflation of pneumatic chambers offers several advantages over traditional fiber-reinforced bending actuators. Specifically, robotic skins made from mechanical metamaterials can be easily applied to or removed from soft robots as needed, allowing for flexibility in design iterations, repairs, or customization [32]. Enclosing soft robots with metamaterial-inspired skins provides design flexibility to achieve a wide range of programmable bending behaviors and even morphing shape designs. Hasse and Mauser [33] proposed a concept that leverages an asymmetrically distributed Poisson's ratio using cellular mechanical metamaterial to enable bending of a soft actuator. Pan et al. [34] further extended the concept and developed a computational framework using the finite element method to analyze the impact of key design parameters of auxetic metamaterials on the bending performance of soft actuators. Rafsanjani et al. [35] introduced buckling-induced Kirigami metamaterials by creating arrays of cuts in thin polyester sheets. These Kirigami metamaterials were later employed as robotic skins to enable soft actuators to crawl [36]. Subsequent studies revealed that stretching Kirigami skins induces elastic instabilities in the thin ligaments, creating a 3D textured surface [37,38]. More recently, the use of Kirigami skins on soft actuators has resulted in a novel class of soft robots with programmable functionalities, including bending [39] and shape morphing [40].

Motivated by previous research on programming soft robots with mechanical metamaterials, this paper extends the concept by using auxetic metamaterial-inspired robotic skins to enable complex, programmable bending behaviors in soft pneumatic actuators. Auxetic and honeycomb metamaterials, made from rubber-like materials, are employed as robotic skins not only because their properties can be readily programmed by altering geometric parameters, but also because the arrangement of unit cells in these metamaterial skins provides a wide design space for actuator design. Additionally, unlike thin Kirigami skins, which can experience stress concentrations at the cutout edges leading to potential permanent plastic deformation [35,37], rubber-like auxetic metamaterials are fully elastic, allowing the actuators to recover their original shape without permanent deformation after unloading. Specifically, soft robotic specimens were fabricated, and inflation experiments were conducted to characterize the bending performance of the actuators upon air pumping. Finite element (FE) models were developed and validated against experimental results. Parametric studies were performed to analyze the effect of the mechanical metamaterials' geometric parameters on the bending and hoop expansion behavior of the soft actuators under pressurization. Furthermore, a variety of programmable bending cases were demonstrated through our models, illustrating how complex programmable bending can be achieved with the proposed strategy.

The content is organized as follows: Section 2 outlines the design concept of the auxetic metamaterial-inspired robotic skins and the geometric design of the bending actuator. Section 3 describes the fabrication and experimental methods, as well as the FE techniques utilized to characterize the deformation of the soft bending actuators. Section 4 presents the experimental and numerical results of the bending performance characterization of the actuators, and compares the parametric study results to reveal the effect of key design parameters of the metamaterial skin on the longitudinal bending and hoop expansion behaviors of the actuators. Several examples are also presented to demonstrate the potential of the proposed concept in designing programmable bio-inspired bending and curved shape-morphing capabilities. Finally, Section 5 summarizes the findings of the study and provides outlooks for future research.

2. Auxetic metamaterial-inspired robotic skins for soft pneumatic actuators

Fig. 1 depicts the fundamental idea considered in this work, which involves leveraging auxetic metamaterials as a robotic skin to induce asymmetric deformation in pneumatic actuators. This concept was initially proposed by Hasse et al. [33] and subsequently investigated by Pan et al. [34] and other researchers [41,42]. However, previous investigations have focused on demonstrating simple bending of the actuators. In this work, we advance these designs to attain programmable bio-inspired bending and curved shape-morphing by exploring additional facets of the design space.

Fig. 1A depicts the unit cell of a negative Poisson ratio (NPR) metamaterial side by side with that of a positive Poisson ratio (PPR) metamaterial, along with their interconnection. Each unit cell is characterized by its width w, height h, the gap distance g. The cross-section of the beam is rectangular with width a and thickness b. A ratio of the gap distance to the height of the unit cell, denoted as $c_g = g/h$, is defined to quantify the geometric variations of the unit cell. A comprehensive depiction of the beam thickness of the unit cell is provided in the Supplementary Information, as illustrated in Fig. S1. A finite-sized mechanical metamaterial is created by replicating the unit cells horizontally for n_h times and vertically for n_v times. Subsequently, it is rolled into a cylindrical shell configuration, resulting in the formation of a robotic skin, which is characterized by the longitudinal length L and the radius of the cross-sectional circle R, as can be seen in Fig. 1B. Subsequently, the metamaterial-based robotic skin is utilized to encompass a thin-walled soft tube, with a thickness of t, to form an integrated pneumatic actuator, as depicted in Fig. 1C. Upon pumping air into the pneumatic cavity, the soft actuator expands radially and elongates longitudinally. Notably, due to the difference between the stretchability of the NPR metamaterial (highlighted in blue) compared to the PPR metamaterial (highlighted in red), the elongation on the NPR side surpasses that on the PPR side. Consequently, this imbalance in elongation results in bending towards the PPR side, as illustrated in the left panel of Fig. 1D. The middle and right panels of Fig. 1D show that by designing the arrangement of the NPR and PPR metamaterials within the robotic skin, complex programmable bending can be achieved.

3. Methodology

3.1. Experiments

Fig. 2 illustrates the fabrication process of the auxetic metamaterial-enabled soft pneumatic actuators. The inner soft tube was fabricated via an injection molding process, with Fig. 2A displaying the 3D printed mold made of resin (8200Pro, Wenext Technology, China) used for fabrication. Equal amounts of Ecoflex 00-30 A and B (Smooth-On, USA) were measured and mixed in a clean container. The mixture was then poured into the mold, as depicted in Fig. 2B, and placed in a blast drying oven at a temperature of 75 °C for 15 minutes to cure. Once the silicone had fully cured, it was removed from the mold and fastened to 3D-printed resin components at its ends to form an enclosed soft tube, as depicted in Fig. 2C. In the meantime, the auxetic metamaterial-inspired robotic skin was fabricated using a separate injection molding process, employing polyurethane-based rubber (Hei-Cast 8400, WeNext Technology, China) as the raw material. Finally, the fabricated robotic skin

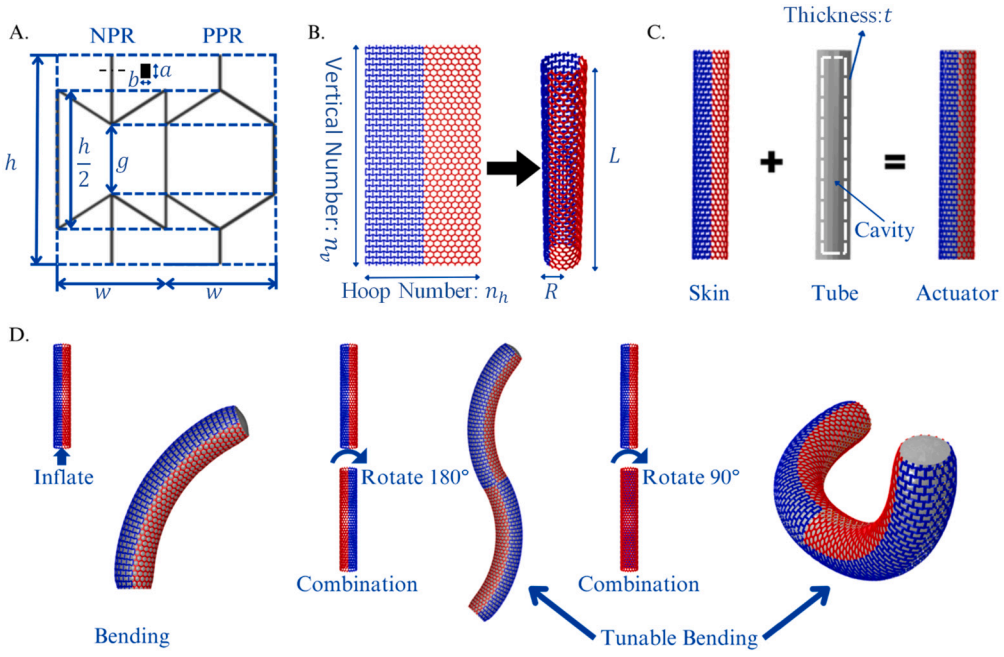

Fig. 1. Auxetic metamaterials act as a robotic skin to enable programmable bending of soft pneumatic actuators. (A) The schematic depicts a negative Poisson ratio (NPR) unit cell, a positive Poisson ratio (PPR) unit cell, and their connection. (B) The unit cells are repeated to form a finite-sized metamaterial, which is then rolled into a cylindrical shell shape, resulting in a robotic skin. (C) The robotic skin is applied to enclose a thin-walled soft tube to create a pneumatic actuator. (D) When air is pumped into the inner soft tube, the asymmetric deformation induced by the robotic skin causes the actuator to bend. Complex programmable bending can be achieved via rigorous design of the metamaterial skin.

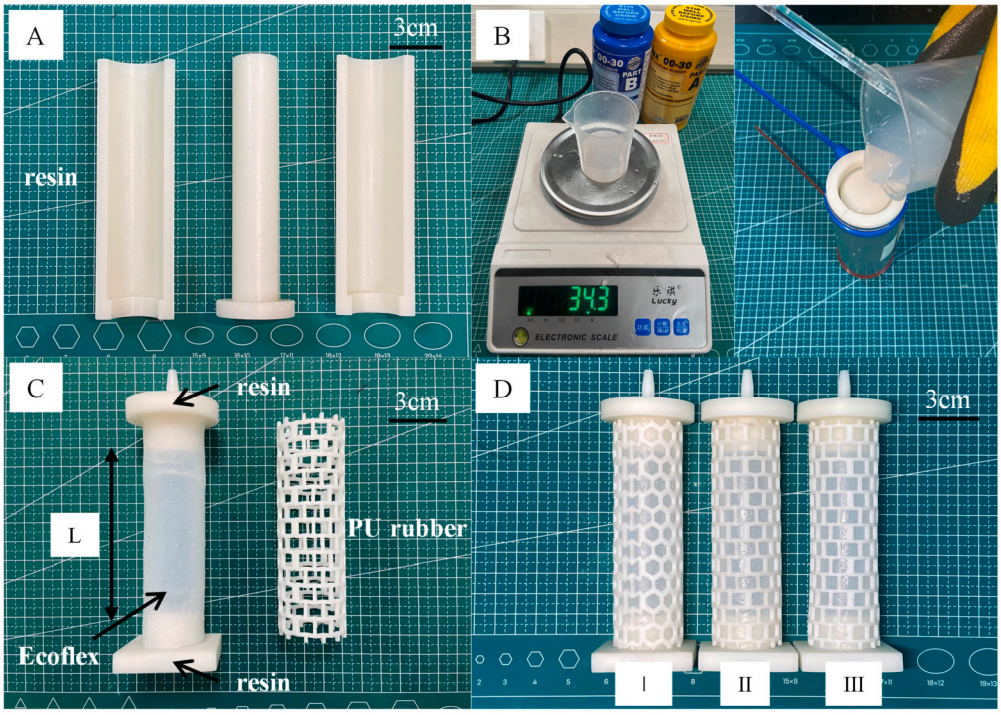

Fig. 2. Fabrication of the auxetic metamaterial-enabled soft bending actuator. (A) 3D printed resin mold for the fabrication of the inner soft tube. (B) Ecoflex 00-30 A and B are mixed and poured into the mold for curing. (C) The cured soft tube is inserted with 3D-printed components at both ends to create an enclosed pneumatic actuator. The robotic skin is fabricated using a separate injection molding process, utilizing polyurethane (PU)-based rubber as the raw material. (D) The soft tube and the robotic skin are adhered together to produce a bending actuator. Three specimens are characterized by different geometric parameters.

and the soft tube were assembled to form the pneumatic actuators. Three specimens, denoted as Specimen-I, II, and III, with variations in the geometric design of the metamaterial skin, were manufactured, as depicted in Fig. 2D. Table 1 summarizes the geometric parameters for the specimens.

The Ecoflex used for the inner tube and the polyurethane-based rubber used for the outer robotic skin were characterized through standard mechanical tests (ASTM D412), yielding a tensile modulus of 0.111 MPa and 5.55 MPa, respectively. Next, experiments were carried out to measure the bending deformation of the pneumatic actuator upon controlled

Table 1
Geometric parameters for the auxetic metamaterial-inspired bending actuator.

	Geometric Parameters	Definition	Value	Unit
Unit Cell	Height of unit cell	h	14.9	mm
	Width of unit cell	w	8.12	mm
	Ratio of gap distance to height	$c_g = g/h$	0.2, (0.4, 0.5)	/
	Beam cross-section parameter, depth	a	2.0	mm
	Beam cross-section parameter, width	b	1.57	mm
Robotic skin	Longitudinal length	L	104.3	mm
	Inner Radius	R	14.5	mm
	Number of unit cells in vertical direction	n_v	7, (5, 9)	/
	Number of unit cells in hoop direction	n_h	12, (16, 20)	/
Inner tube	Thickness	t	2.0	mm

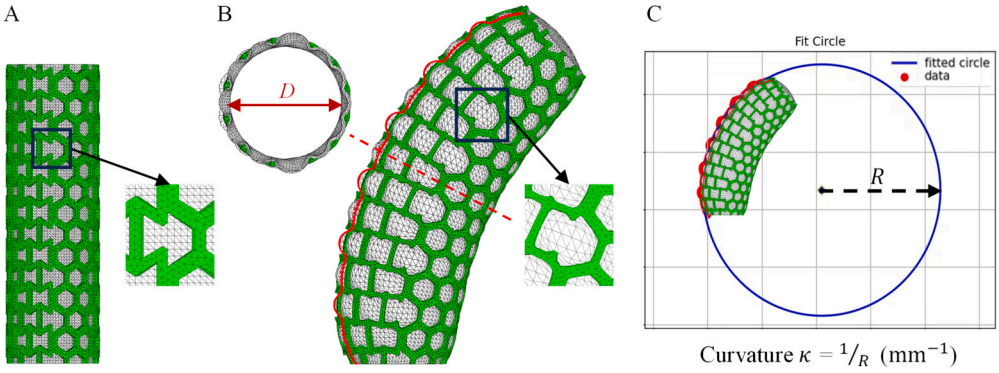

Fig. 3. Finite element mesh representation of the auxetic metamaterial-enabled soft actuator. (A) Initial configuration. (B) Deformed configuration. (C) Measurement of the bending curvature.

air pumping. A detailed description of the experimental set-up can be found in Section II of the Supplementary Information.

3.2. Model

To comprehend the bending mechanics and guide the design of the actuator, numerical models were constructed utilizing the commercial finite element package ABAQUS/Standard 2020. Fig. 3 illustrates the finite element mesh of the actuator in the initial and deformed configuration. Both the robotic skin and the inner tube were discretized using three-dimensional quadratic tetrahedral elements with hybrid formulation (ABAQUS element type: C3D10H). The mesh density accuracy was ensured through a mesh refinement study. The nonlinear behaviors of both the robotic skin and the inner tube were modeled using an incompressible Neo-Hookean material model, with the initial shear modulus of 0.037 MPa and 1.85 MPa, respectively. The bottom end of the actuator was completely constrained. The model was inflated via a fluid cavity interaction within ABAQUS. The fluid was modeled as incompressible air with a density of 1.225 kg/m^3. The inflation process was controlled by gradually adding air volume to the cavity, which was simulated by introducing a fictitious thermal expansion and applying a temperature change load to the air. The added air volume is related to the temperature change through the following equation:

$$\Delta V = V_0 \cdot 3\alpha\Delta T \tag{1}$$

where ΔV represents the change in fluid cavity volume, V_0 denotes the initial volume of the cavity, α is the coefficient of thermal expansion of the fluid, and ΔT is the temperature change. The deformation of the soft actuator upon inflation was captured using the dynamic implicit solver, and the quasi-static condition was ensured by monitoring the kinetic energy of the model to be a small percentage of its strain energy. Fig. 3B illustrates the deformation of the mesh in the inflated state of the actuator. The cross-section diameter, D, at the middle length of the actuator is extracted to measure the hoop expansion of the actuator. The coordinates of the nodes located along the outer edge (highlighted with a red line) are extracted and exported to a circle-fitting Python code [43] for the measurement of the bending curvature, κ, as shown in Fig. 3C. We note that the outer edge was selected to quantify the bending of the actuator because the inner edge experiences convex and concave variations along its length due to constraints at the actuator's ends, making it challenging to accurately fit the curve into a circle, especially when the actuator is short and boundary effects are pronounced.

4. Results and discussion

4.1. Bending responses of the actuators

In this section, we start by characterizing the bending responses of the proposed auxetic metamaterial-inspired soft actuators under air pumping. Fig. 4 presents a comparison between experimental observations and numerical simulations, demonstrating a high level of agreement. As mentioned above, three specimens were fabricated and tested to highlight the influence of asymmetry in the geometry of the metamaterial skin on bending performance of the actuators. These specimens are characterized by a range of c_g values, specifically $c_g = 0.2$, 0.4, and 0.5 for Specimen-I, -II, and -III, respectively. Note that a smaller value of c_g results in a more significant asymmetry between the NPR and PPR metamaterials, whereas $c_g = 0.5$ denotes the adoption of a symmetric design. Numerical models with identical geometric dimensions were developed and executed to capture the deformation of these actuators. Fig. 4A illustrates the comparison of inflation pressure as a function of increased air volume for the three specimens. It is evident that as air is pumped into the actuator, the inflation pressure of the cavity increases, and the pressure at the same increased air volume is close to each other for all three specimens. Figs. 4B and 4C present the bending curvature of the actuator as a function of inflation pressure and increased air volume, respectively. It can be seen that the bending curvature of the actuator increases as the pneumatic cavity is inflated. Fig. 4D presents deformation

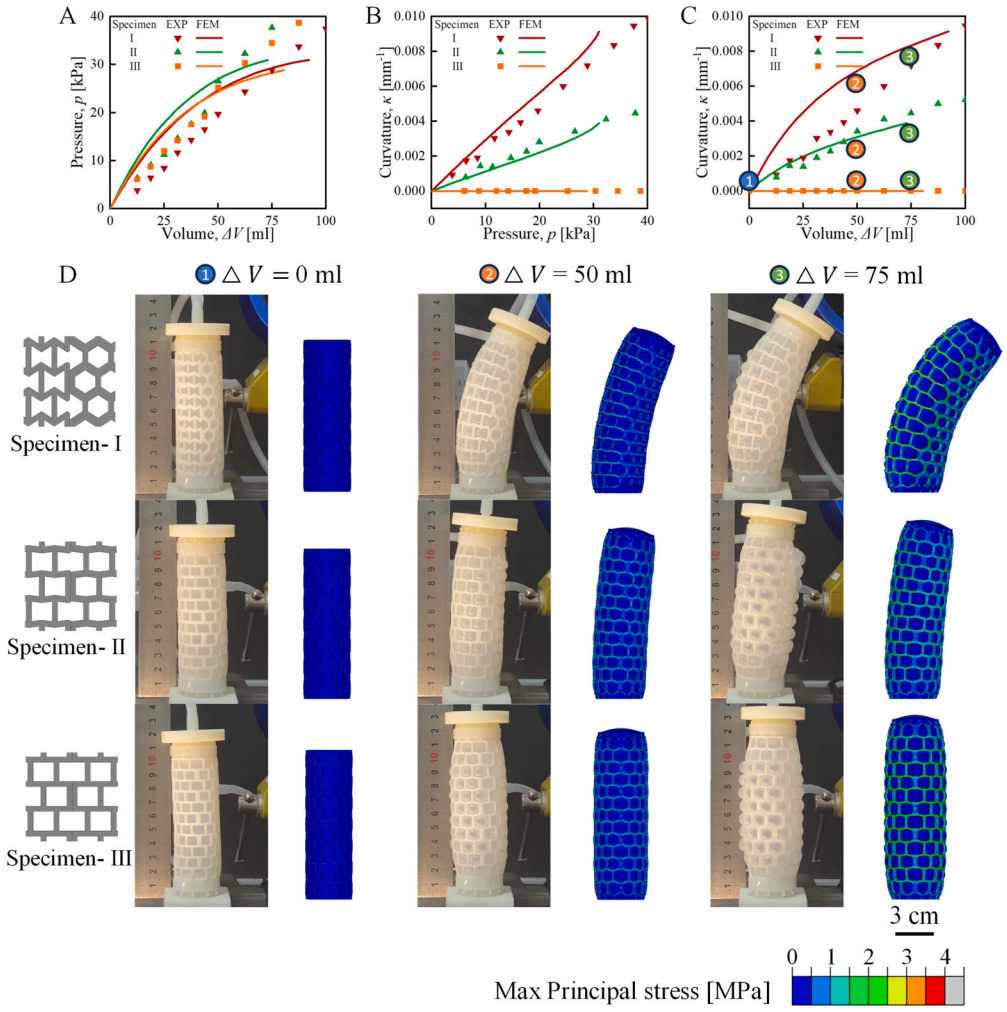

Fig. 4. Bending response of three auxetic metamaterial-inspired soft actuators subjected to air pumping. Comparison between experimental and numerical results for (A) pressure versus volume, (B) bending curvature versus pressure, (C) bending curvature versus volume curves, and (D) deformation snapshots.

snapshots obtained from both experiments and simulations, demonstrating a close match between the two. A movie showing the deformation animations of both the experiment and simulation can be found in the Supplementary Information, available as Movie S1. It can be observed from the movie that localized bulging occurs in the soft inflatable tube. This is due to the high nonlinearity and thin-walled nature of the tube material. However, this bulging effect was not well captured in our simulations, as we used the Neo-Hookean model for the analysis. To capture such bulging behavior, more advanced hyperelastic material models, such as the Gent or Ogden models, would be required, as they better account for the high nonlinearity of rubber materials [6,44,45]. In this work, the Neo-Hookean model was selected because it efficiently captures the bending behavior of the actuator while reducing computational costs, as bulging is not the primary focus of this study.

We note that the bending of the actuator is attributed to the asymmetric constraint imposed by the robotic skin, where the Poisson effect of the auxetic metamaterial is pivotal. Upon inflation of the inner tube, it applies uniform expansion forces on the outer metamaterials in both the longitudinal and hoop directions. The mechanical behavior of the outer metamaterial has been elucidated through FE simulations, as elaborated in the Supplementary Information (refer to Fig. S3). In the longitudinal direction, the NPR metamaterial on the left exhibits much lower tension stiffness compared to the right PPR metamaterial. Thus, under the actuation force exerted by the inner tube, the left side of the actuator exhibits longer elongation than the right side. Additionally, owing to the Poisson effect, expansion in the hoop direction on the left side induces longitudinal elongation, whereas expansion in the hoop direction on the right side induces longitudinal shortening. Consequently, upon inflation, the left side of the actuator experiences significantly more elongation than the right side, resulting in bending towards the right side. It is further demonstrated that the bending performance of the actuator can be readily adjusted by varying the geometric parameter c_g of the metamaterial skin. Specifically, Specimen-I ($c_g = 0.2$) displays a more pronounced asymmetry between the left and right sides compared to Specimen-II ($c_g = 0.4$). Consequently, at the same inflation volume and pressure, Specimen-I exhibits a larger bending curvature than Specimen-II. In contrast, Specimen-III ($c_g = 0.5$) features a symmetric skin design, resulting in no bending, and is fabricated and analyzed for comparative purposes.

4.2. Parametric studies

Having demonstrated the bending performance and verified the accuracy of the numerical simulations, we then move on to use our model to explore the effect of key design parameters of the metamaterial-inspired skin on the bending performance of the soft actuators. The geometric parameters outlined in Table 1 are used as a baseline for comparison.

4.2.1. Effect of number of unit cells in vertical direction

We begin by investigating the effect of the number of unit cells used in the vertical direction. Three simulation cases are considered with

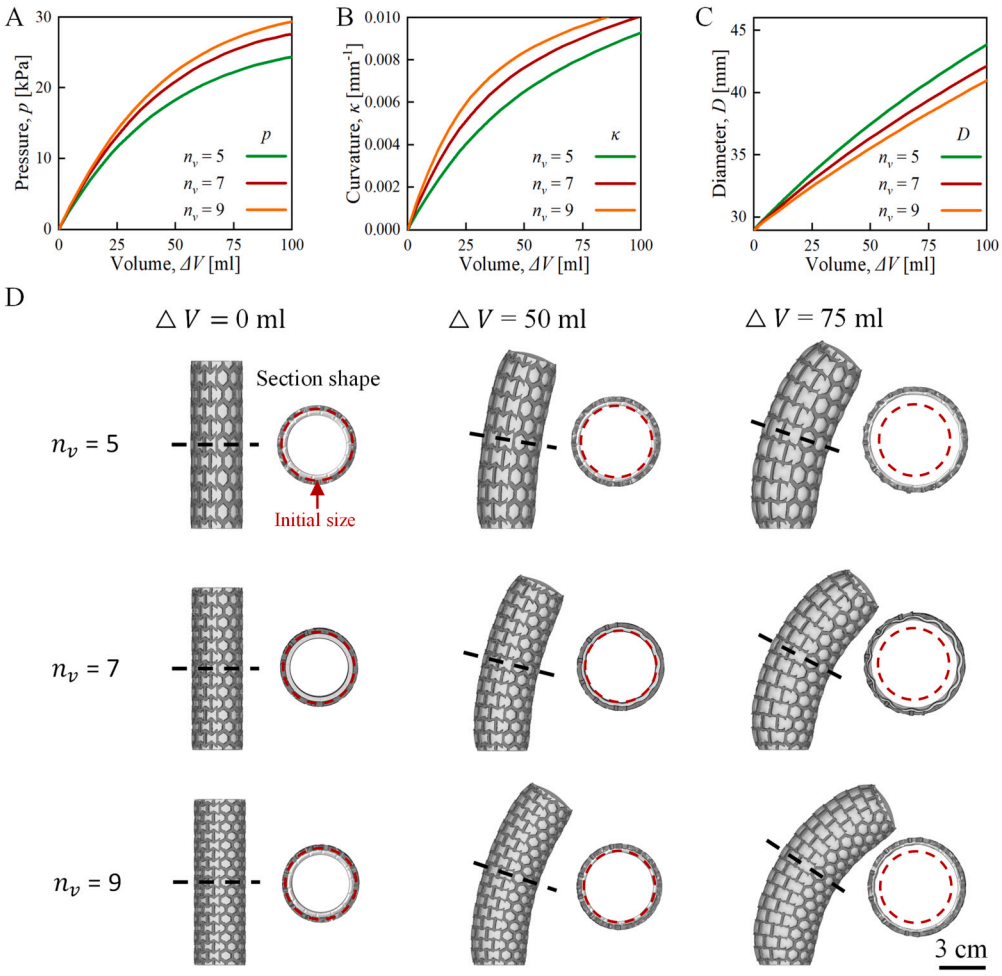

Fig. 5. Effect of the number of unit cells in the vertical direction, denoted as n_v, on the bending performance of the soft actuators. As n_v increases, (A) the inner pressure exerted on the soft actuator and (B) the bending curvature of the actuator increase at the same inflation volume. On the contrary, (C) the cross-sectional diameter of the actuator decreases.

identical design parameters, except for the number of unit cells in the vertical direction, n_v, which varies from 5, 7, to 9.

Fig. 5 shows the simulation results. The results indicate that as n_v increases, the bending curvature along the longitudinal direction of the actuator increases, while the expansion in the hoop direction decreases. This can be attributed to the variation in the mechanical properties of the outer metamaterials, as detailed in the Supplementary Information (see Fig. S4). As n_v increases, both the NPR and PPR metamaterials experience a reduction in tension stiffness in the longitudinal direction. Consequently, for a larger n_v, the actuator overall has reduced stiffness in the longitudinal direction, making it easier to elongate. Additionally, as n_v increases, the expansion in the hoop direction causes a larger elongation in the longitudinal direction for the left NPR and, simultaneously, a larger shortening for the right PPR. Consequently, with increasing n_v, the actuator exhibits a more significant difference between the elongation of the left and right sides, resulting in a larger bending curvature. On the other hand, as n_v increases, both the NPR and PPR metamaterials experience an increase in tension stiffness in the hoop direction, resulting in relatively large stiffness in this direction to limit the expansion of the actuator. Moreover, as n_v increases, the elongation in the longitudinal direction causes a decrease in the expansion in the hoop direction for the left NPR, while for the right PPR, the Poisson effect remains almost unchanged. Consequently, with increasing n_v, the expansion in the hoop direction of the actuator is limited

4.2.2. Effect of number of unit cells in hoop direction

Next, we explore the effect of the number of unit cells used in the hoop direction. Three simulation cases are considered with identical design parameters, except for the number of unit cells in the hoop direction, n_h, which varies from 12, 16, to 20.

Fig. 6 shows the bending simulation results. The results indicate that as n_h increases, the bending curvature along the longitudinal direction of the actuator slightly decreases, while the expansion in the hoop direction significantly increases. This can be attributed to the variation in the mechanical properties of the outer metamaterials, as detailed in the Supplementary information (see Fig. S5). As n_h increases, both the NPR and PPR metamaterials experience an increase in tension stiffness in the longitudinal direction. Consequently, for a larger n_h, the actuator overall has an increased stiffness in the longitudinal direction, making it harder to elongate. Additionally, as n_h increases, the expansion in the hoop direction causes a less pronounced elongation in the longitudinal direction for the left NPR and, simultaneously, a less pronounced shortening for the right PPR. Consequently, with increasing n_h, the actuator exhibits a much less difference between the elongation of the left and right sides, resulting in a smaller bending curvature. On the other hand, as n_h increases, both the NPR and PPR metamaterials experience a decrease in tension stiffness in the hoop direction, resulting in relatively small stiffness in this direction to limit the expansion of the actuator. Moreover, as n_h increases, the elongation in the longitudinal direction causes an increase in the expansion in the

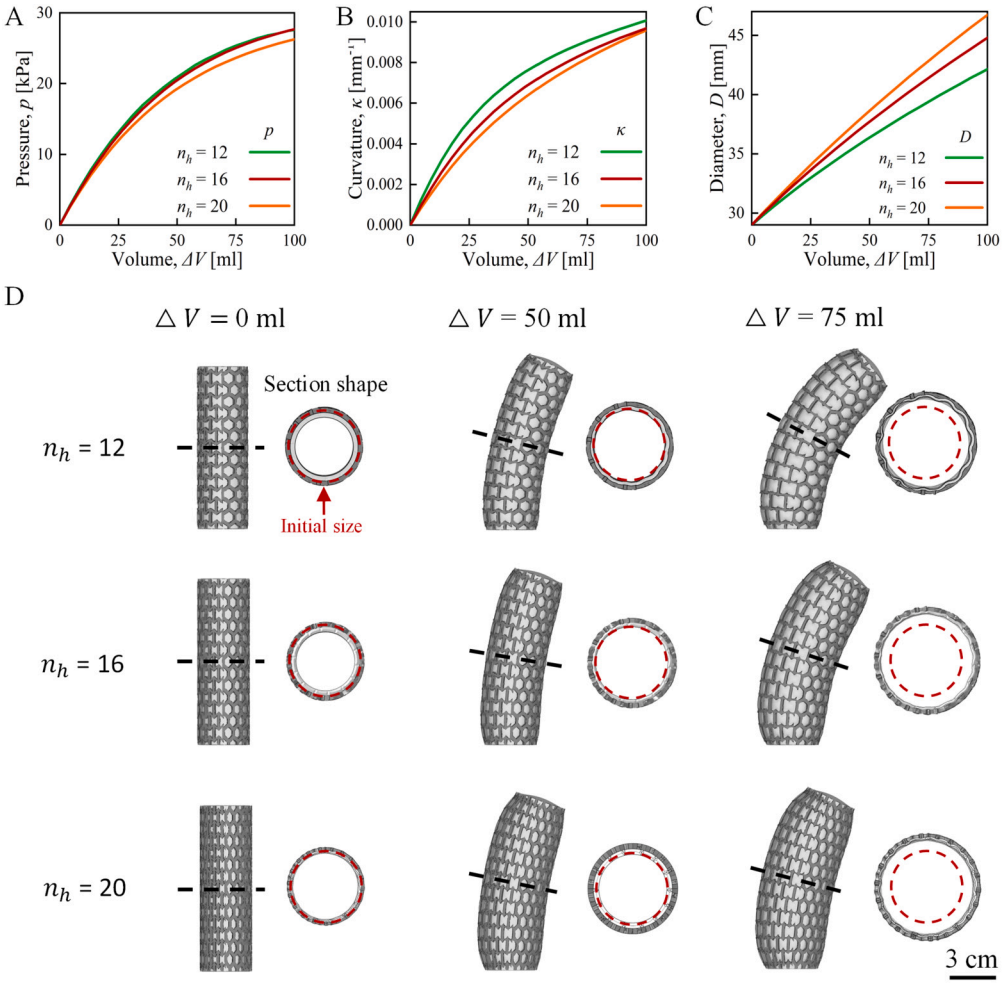

Fig. 6. Effect of the number of unit cells in the hoop direction, denoted as n_h, on the bending performance of the soft actuators. As n_h increases, (A) the inner pressure exerted on the soft actuator increases slightly and (B) the bending curvature of the actuator decreases slightly at the same inflation volume. Meanwhile, (C) the cross-sectional diameter of the actuator increases significantly.

hoop direction for the left NPR. Consequently, with increasing n_h, the expansion in the hoop direction of the actuator becomes much more prominent.

4.2.3. *Effect of modulus ratio of metamaterial to inner tube*

In this section, we investigate the effect of the modulus ratio between the metamaterial and the inner soft tube on the bending performance of the actuator. We consider three simulation cases with identical geometric parameters as listed in Table 1. In these simulations, the initial shear modulus of the inner tube is fixed at a constant value of 0.037 MPa, while that of the outer skin varies to achieve different modulus ratios of the outer metamaterial to the inner tube, denoted as α, ranging from 20, 50, to 80.

The bending simulation results are presented in Fig. 7. The results suggest that the modulus ratio has a negligible effect on the bending curvature and the hoop expansion of the actuator. However, it does provide an effect on the inflation pressure-to-volume curve. As the modulus of the skin material increases, both the left NPR and the right PPR metamaterials become stiffer, resulting in an overall increase in stiffness in all directions for the actuator. However, the Poisson effect of the NPR and PPR metamaterials remains almost unchanged, see Fig. S6 in the Supplementary Information. Therefore, we can conclude that the Poisson effect of the auxetic metamaterial, as well as the asymmetry between the left and right sides, is the main reason for the bending of the actuator.

4.2.4. *Combined parameter effects*

Fig. 8 illustrates the combined effect of varying the number of unit cells in the hoop and vertical directions on the actuator's performance. The results are obtained with a constant inflation volume of 75 mL. The color contour and isolines reveal that increasing the number of unit cells in the vertical direction while decreasing the number of unit cells in the hoop direction enhances bending performance by increasing bending curvature while constraining hoop expansion. For example, the bending curvature (κ) increases from 0.0077 mm^{-1} to 0.0097 mm^{-1}, while the cross-section diameter (D) decreases from 44.0 mm to 38.4 mm when the number of unit cells in the vertical direction is increased from n_v = 5 to n_v = 9 and the number of unit cells in the hoop direction is decreased from n_h = 20 to n_h = 12.

Additionally, we investigated the effect of varying the fraction of NPR unit cells in the hoop direction while keeping the total number of unit cells constant. In these simulations, we maintained identical geometric and material parameters as listed in Table 1, with the only variable being the fraction ratio of NPR unit cells. With the total number of hoop direction unit cells fixed at 12, we increased the number of NPR unit cells from 0, 2, 4, 6, 8, 10 to 12, thereby raising the fraction ratio from 0 to 1. As shown in Fig. 9, when the actuator is inflated to 25 kPa, the hoop expansion increases monotonically with the increasing fraction of NPR. However, the bending curvature initially rises, peaks when the NPR fraction ratio is 0.5 (where NPR and PPR unit cells are equal in number), and then decreases.

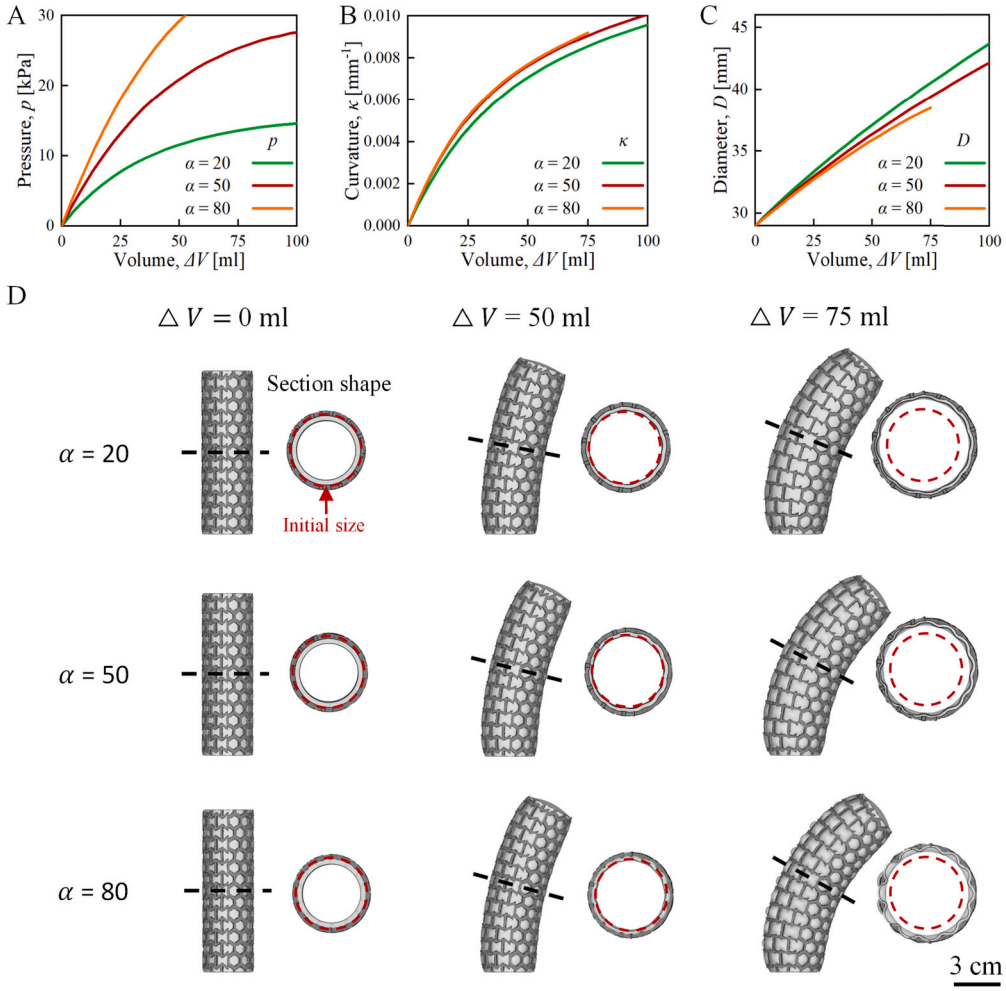

Fig. 7. Effect of the ratio of the initial shear modulus of the outer skin to the inner soft tube, denoted as α, on the bending performance of the soft actuators. It is observed that (A) the inner pressure exerted on the soft actuator increases significantly, while (B) the bending curvature, and (C) the cross-sectional diameter of the actuator remain almost unchanged as α increases.

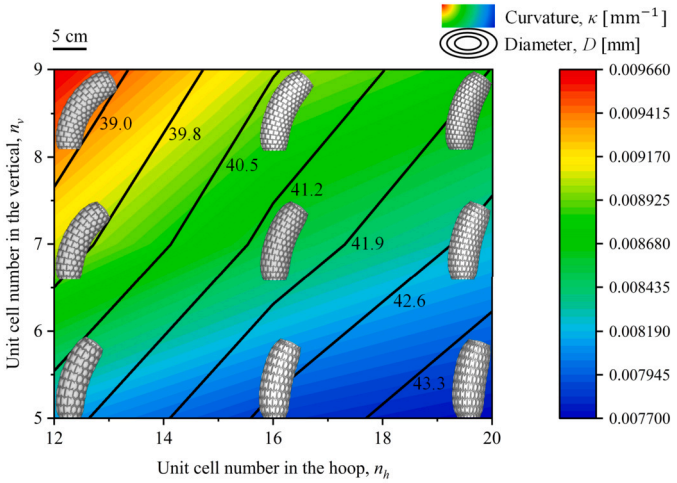

Fig. 8. Combined effect of unit cell numbers in the hoop and vertical directions. The color contour represents bending curvature variation, while the isolines indicate cross-section diameter changes.

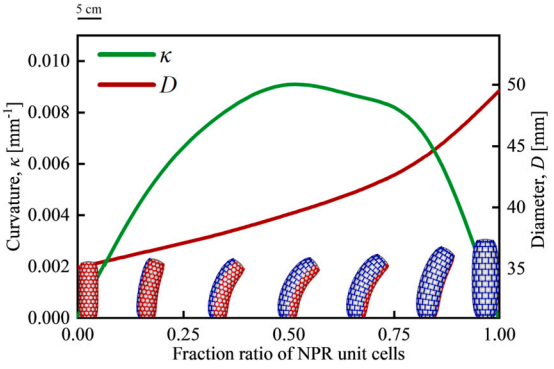

Fig. 9. Effect of the fraction of NPR unit cells on bending performance of the soft actuators. As the fraction of NPR unit cells increases, hoop expansion rises steadily, while bending curvature initially increases, peaks, and then decreases. Blue and red respectively indicate NPR and PPR unit cells in the color demonstration.

4.3. Programmable bending

Having understood that adjusting the geometric parameters and the number of unit cells in the longitudinal and hoop directions facilitates the creation of soft actuators with customizable bending curvature and hoop expansion, we then explore the potential of using this concept to program more complex bio-inspired bending and curved shape-morphing behaviors. To illustrate this idea, in this section, we present several designs that mimic bio-inspired bending motions and customized English characters as examples. All geometric

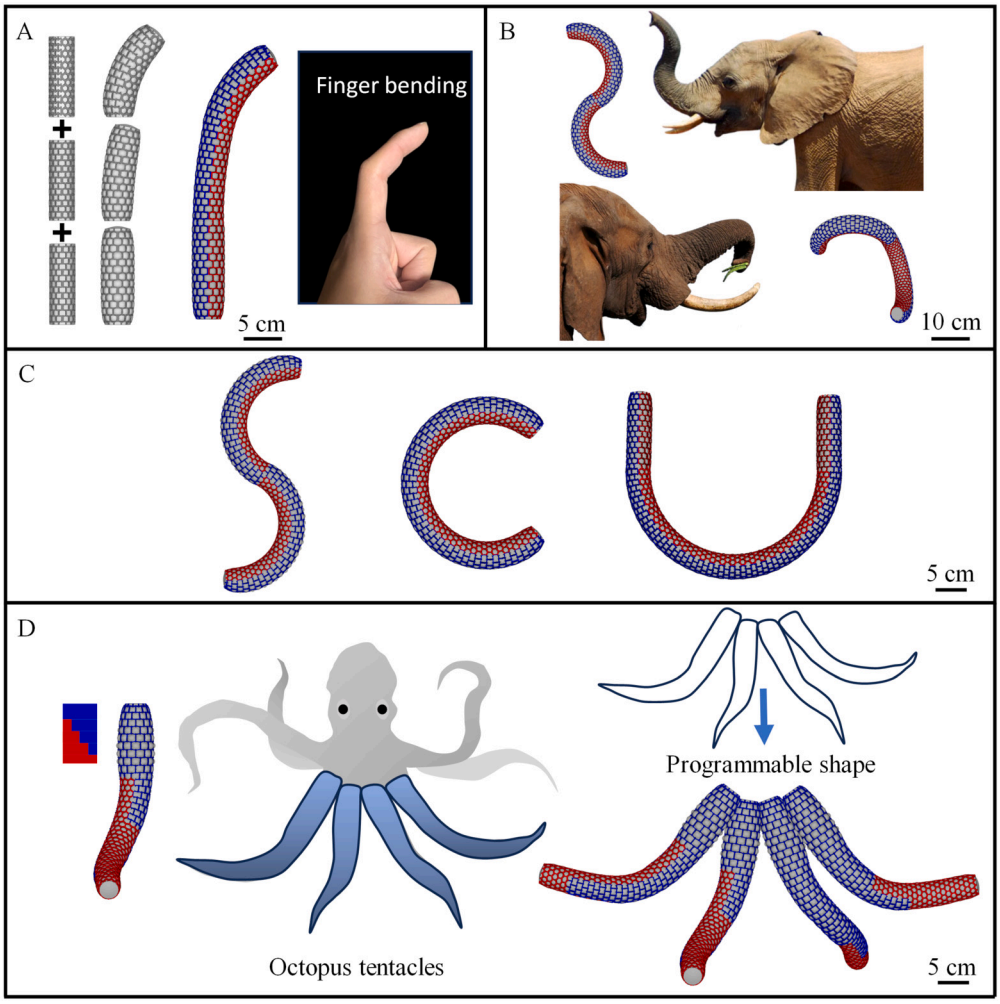

Fig. 10. Demonstration of a variety of programmable bending actuators achieved with specialized metamaterial skins. (A) A soft robot resembling the bending motion of a human finger. (B) A soft robot emulating the complex bending and twisting of an elephant's trunk. (C) Three soft actuators forming the English characters "S", "C", and "U", where "SCU" represents SiChuan University, showcasing customized shape morphing capabilities. (D) A soft robot imitating the intricate bending of octopus tentacles.

design details are shown in Figs. S7-S12 in the Supplementary Information.

Fig. 10A illustrates a soft robot that replicates the bending motion of a human finger. This is achieved by connecting three segments of the actuators in series, with varying bending curvatures along the longitudinal direction achieved by using three different c_g values. Fig. 10B illustrates a soft actuator designed to replicate the complex bending and twisting motions of an elephant's trunk. This is accomplished by incorporating a metamaterial skin composed of two segments, each featuring a distinct distribution of NPR and PPR unit cells. Fig. 10C showcases three soft actuators configured to form the English characters "S", "C", and "U", representing the abbreviation for SiChuan University. These examples highlight the versatility of the method in achieving customized shape-morphing capabilities. Fig. 10D depicts a soft actuator replicating the intricate bending of octopus tentacles. The actuator initially has a cylindrical shape, which transforms into a twisting conical form under inflation. This transformation is achieved by adjusting both the hoop expansion and the bending curvature of the actuator. As depicted in Fig. S12 in the Supplementary Information, the metamaterial skin for the octopus tentacle actuator is composed of multiple segments where at the top consists of all NPR unit cells, while at the bottom consists of all PPR unit cells. Along the axial direction, the number of NPR cells gradually decreases, and the number of PPR cells increases, while the total number of unit cells in the hoop direction remains constant. This gradient design results in varying degrees of hoop expansion along the axial direction, with an overall decrease in hoop expansion from the top to the bottom of the tentacle. Additionally, bending is introduced in the middle section of the actuator, with variations in bending curvature arising from the varying fraction of NPR unit cells.

Finally, Figs. S7-S12 in the Supplementary Information illustrate the maximum principal stress distribution for all demo samples. Notably, the NPR side experiences higher stress due to greater elongation, and the actuator predictably bends from NPR to PPR, showing that bending can be easily tuned by adjusting the unit cell arrangement. The consistent maximum principal stress at segment intersections indicates smooth transitions without stress concentration, suggesting that the complex bio-inspired actuators likely exhibit similar functionality to the simpler bending actuators. We note that the maximum principal stress in the inner tube and metamaterial skin for the samples, as shown in Figs. S7-S12, ranges from 0.4 to 0.6 MPa and 4.0 to 6.0 MPa, respectively. These stress values are well below the failure stresses of the respective materials-1.38 MPa for Ecoflex 00-30 [46] and 10 MPa for Hei-Cast 8400 [47]. This suggests the actuator is likely capable of withstanding cyclic loading. However, a comprehensive assessment of long-term performance under cyclic conditions would require additional fatigue studies, including detailed durability tests [16,48], which is however beyond the scope of this work.

5. Conclusion

Bending serves as a fundamental deformation mode essential for achieving complex motions in soft robots. In the realm of pneumatic soft robots, various design methods have been proposed to facilitate bending. These methods can be broadly categorized into two groups: the first involves employing asymmetric material or geometric distributions to induce bending of the actuator, while the second entails incorporating reinforcements to introduce asymmetric constraints, such as fiber-reinforcement, knit fabrics, and mechanical metamaterials. Of these, mechanical metamaterial-inspired robotic skins have garnered attention for their ease of use and removal, as well as their capacity for offering significant design flexibility.

This paper investigates the concept of using auxetic metamaterial-inspired robotic skin to program the bending behavior of pneumatic soft actuators. The idea is intuitive. The robotic skin comprises a combination of NPR metamaterial and PPR metamaterial, while the inner tube consists of a cylindrical thin-walled soft chamber made of rubber-like soft materials. Upon inflation with air, the NPR and PPR metamaterials cause differential elongation on the actuator's sides, resulting in directional bending. Experiments and finite element simulations are employed to analyze the bending deformation of the actuators, with the simulations validated against experimental results. Parametric studies are conducted to explore the influence of key design parameters on actuators' bending performance. The main findings are summarized as follows: *(i)* Bending curvature can be increased and hoop expansion can be reduced by increasing the unit cell numbers in the vertical direction while decreasing the unit cell numbers in the hoop direction. *(ii)* The modulus ratio of the metamaterial to the inner tube has a significant effect on the pressure-volume relationship of the actuator but has a negligible effect on bending performance. Furthermore, the concept is demonstrated to enable complex bio-inspired programmable bending and curved shape-morphing by altering the heterogeneous distribution of NPR and PPR materials. A series of design examples are presented for demonstration.

In conclusion, this paper provides new insights into leveraging metamaterials for soft robotic design, with promising applications in bio-inspired soft robotics, including grasping, crawling, and more. Future research can explore several key directions:

Unit cell design: The design of unit cells for the robotic skin can be enhanced by incorporating novel configurations where stiffness and Poisson's ratio are programmable as functions of applied strains through self-contact mechanisms [49,50]. This approach holds potential to enable the programming of the morphing shape evolution of pneumatic actuators simply through controlled inflation, allowing for precise manipulation of shape changes during the inflation process.

Experimental Techniques: The design principles revealed through our FEM simulations are expected to be applicable across a wide range of length scales, from millimeters to meters, due to the inherent scale invariance of the FEM models. This scale invariance arises because the bending behavior of the actuator is primarily dictated by the differences in stiffness and Poisson's ratio between the NPR and PPR metamaterials of the robotic skin, which are determined by the microstructural geometry rather than the material composition. As long as the stiffness ratio between the robotic skin and the inflatable tube remains within the reasonable range discussed in the paper, the actuator's mechanical behavior remains consistent irrespective of scale. Consequently, programming the performance of the soft actuators depends on the high-quality manufacture precision of the microstructural geometry of the metamaterial skins. Although the molding and casting method employed in this paper limits the size of the actuators that can be fabricated, advanced manufacturing techniques, such as Digital Light Processing (DLP) and Fused Deposition Modeling (FDM), can be employed to fabricate both miniature and larger soft robots that conform to the proposed design principles [51–53], thereby broadening the versatility and applicability of our approach across various soft robotic systems.

Simulation and Optimization: In terms of simulations, this paper focuses on developing high-fidelity 3D FEM models to accurately capture the bending behavior of the actuators and to demonstrate the efficiency of using auxetic metamaterials as robotic skins for bending actuators. We acknowledge that future work could explore achieving complex programmable morphing behaviors in pneumatic actuators through an inverse optimization framework, which would require numerous simulations to design the geometric parameter distribution of the robotic skins [40]. For such problems, homogenization of the unit cell and multiscale analysis hold potential for enhancing computational efficiency [54]. Specifically, homogenization can be used to determine effective macroscopic properties, such as anisotropic stiffness and Poisson's ratio, of the unit cell. These properties can then be employed to model the robotic skin as a homogeneous material, thereby reducing computational costs while maintaining accuracy.

CRediT authorship contribution statement

Yichen Pu: Methodology, Investigation. **Shengwei Zheng:** Methodology. **Xinjie Hu:** Validation. **Shan Tang:** Writing – review & editing. **Ning An:** Writing – review & editing, Writing – original draft, Supervision, Project administration, Conceptualization.

Declaration of competing interest

The authors declare that they have no known competing financial interests or personal relationships that could have appeared to influence the work reported in this paper.

Data availability

The finite element codes for reproducing the simulation works presented in the paper can be downloaded from https://github.com/SCU-An-Group/Metamaterial-Skins-for-Soft-Actuators.

Data will be made available on request.

Acknowledgement

This research is supported by the National Natural Science Foundation of China (grant 12202295), the Fundamental Research Funds for the Central Universities, China (grant YJ2021137), and the Open Project of State Key Laboratory of Structural Analysis for Industrial Equipment, Dalian University of Technology (No. GZ22120).

Appendix A. Supplementary material

Supplementary material related to this article can be found online at https://doi.org/10.1016/j.matdes.2024.113334.

References

[1] D. Rus, M.T. Tolley, Design, fabrication and control of soft robots, Nature 521 (7553) (2015) 467–475.
[2] H. Wang, M. Totaro, L. Beccai, Toward perceptive soft robots: progress and challenges, Adv. Sci. 5 (9) (2018) 1800541.
[3] Y. Zhang, P. Li, J. Quan, L. Li, G. Zhang, D. Zhou, Progress, challenges, and prospects of soft robotics for space applications, Adv. Intell. Syst. 5 (3) (2023) 2200071.
[4] W.J. Zheng, N. An, J.H. Yang, J. Zhou, Y.M. Chen, Tough al-alginate/poly (n-isopropylacrylamide) hydrogel with tunable lcst for soft robotics, ACS Appl. Mater. Interfaces 7 (3) (2015) 1758–1764.
[5] J. Shintake, V. Cacucciolo, D. Floreano, H. Shea, Soft robotic grippers, Adv. Mater. 30 (29) (2018) 1707035.
[6] T.J. Jones, E. Jambon-Puillet, J. Marthelot, P.-T. Brun, Bubble casting soft robotics, Nature 599 (7884) (2021) 229–233.
[7] A. Rafsanjani, K. Bertoldi, A.R. Studart, Programming soft robots with flexible mechanical metamaterials, Sci. Robot. 4 (29) (2019) eaav7874.
[8] A. Kotikian, C. McMahan, E.C. Davidson, J.M. Muhammad, R.D. Weeks, C. Daraio, J.A. Lewis, Untethered soft robotic matter with passive control of shape morphing and propulsion, Sci. Robot. 4 (33) (2019) eaax7044.

[9] M. Calisti, M. Giorelli, G. Levy, B. Mazzolai, B. Hochner, C. Laschi, P. Dario, An octopus-bioinspired solution to movement and manipulation for soft robots, Bioinspir. Biomim. 6 (3) (2011) 036002.
[10] P. Karipoth, A. Christou, A. Pullanchiyodan, R. Dahiya, Bioinspired inchworm- and earthworm-like soft robots with intrinsic strain sensing, Adv. Intell. Syst. 4 (2) (2022) 2100092.
[11] M. Cianchetti, C. Laschi, A. Menciassi, P. Dario, Biomedical applications of soft robotics, Nat. Rev. Mater. 3 (6) (2018) 143–153.
[12] N. Vasios, A.J. Gross, S. Soifer, J.T. Overvelde, K. Bertoldi, Harnessing viscous flow to simplify the actuation of fluidic soft robots, Soft Robot. 7 (1) (2020) 1–9.
[13] F. Ilievski, A.D. Mazzeo, R.F. Shepherd, X. Chen, G.M. Whitesides, Soft robotics for chemists, Angew. Chem. (Int. Ed.) (2011).
[14] R.V. Martinez, J.L. Branch, C.R. Fish, L. Jin, R.F. Shepherd, R. Nunes, Z. Suo, G.M. Whitesides, Robotic tentacles with three-dimensional mobility based on flexible elastomers, Adv. Mater. (2013).
[15] Z. Xie, A.G. Domel, N. An, C. Green, Z. Gong, T. Wang, E.M. Knubben, J.C. Weaver, K. Bertoldi, L. Wen, Octopus arm-inspired tapered soft actuators with suckers for improved grasping, Soft Robot. 7 (5) (2020) 639–648.
[16] B. Mosadegh, P. Polygerinos, C. Keplinger, S. Wennstedt, R.F. Shepherd, U. Gupta, J. Shim, K. Bertoldi, C.J. Walsh, G.M. Whitesides, Pneumatic networks for soft robotics that actuate rapidly, Adv. Funct. Mater. 24 (15) (2014) 2163–2170.
[17] R. Baines, S.K. Patiballa, B. Gorissen, K. Bertoldi, R. Kramer-Bottiglio, Programming 3d curves with discretely constrained cylindrical inflatables, Adv. Mater. 35 (26) (2023) 2300535.
[18] F. Connolly, P. Polygerinos, C.J. Walsh, K. Bertoldi, Mechanical programming of soft actuators by varying fiber angle, Soft Robot. 2 (1) (2015) 26–32.
[19] P. Polygerinos, Z. Wang, J.T. Overvelde, K.C. Galloway, R.J. Wood, K. Bertoldi, C.J. Walsh, Modeling of soft fiber-reinforced bending actuators, IEEE Trans. Robot. 31 (3) (2015) 778–789.
[20] F. Connolly, C.J. Walsh, K. Bertoldi, Automatic design of fiber-reinforced soft actuators for trajectory matching, Proc. Natl. Acad. Sci. 114 (1) (2017) 51–56.
[21] H. Kim, H. Na, S. Noh, S. Chang, J. Kim, T. Kong, G. Shin, C. Lee, S. Lee, Y.-L. Park, et al., Inherently integrated microfiber-based flexible proprioceptive sensor for feedback-controlled soft actuators, npj Flex. Electron. 8 (1) (2024) 15.
[22] Z. Wang, P. Polygerinos, J.T. Overvelde, K.C. Galloway, K. Bertoldi, C.J. Walsh, Interaction forces of soft fiber reinforced bending actuators, IEEE/ASME Trans. Mechatron. 22 (2) (2016) 717–727.
[23] L. Ge, F. Chen, D. Wang, Y. Zhang, D. Han, T. Wang, G. Gu, Design, modeling, and evaluation of fabric-based pneumatic actuators for soft wearable assistive gloves, Soft Robot. 7 (5) (2020) 583–596.
[24] L. Cappello, K.C. Galloway, S. Sanan, D.A. Wagner, R. Granberry, S. Engelhardt, F.L. Haufe, J.D. Peisner, C.J. Walsh, Exploiting textile mechanical anisotropy for fabric-based pneumatic actuators, Soft Robot. 5 (5) (2018) 662–674.
[25] Z. Zhang, Y. Long, G. Chen, Q. Wu, H. Wang, H. Jiang, Soft and lightweight fabric enables powerful and high-range pneumatic actuation, Sci. Adv. 9 (15) (2023) eadg1203.
[26] A. Bhat, S.S. Jaipurkar, L.T. Low, R.C.-H. Yeow, Reconfigurable soft pneumatic actuators using extensible fabric-based skins, Soft Robot. 10 (5) (2023) 923–936.
[27] K. Bertoldi, V. Vitelli, J. Christensen, M. Van Hecke, Flexible mechanical metamaterials, Nat. Rev. Mater. 2 (11) (2017) 1–11.
[28] X. Zheng, K. Uto, W.-H. Hu, T.-T. Chen, M. Naito, I. Watanabe, Reprogrammable flexible mechanical metamaterials, Appl. Mater. Today 29 (2022) 101662.
[29] E. Medina, C.H. Rycroft, K. Bertoldi, Nonlinear shape optimization of flexible mechanical metamaterials, Extreme Mech. Lett. 61 (2023) 102015.
[30] S. Sun, N. An, G. Wang, M. Li, J. Zhou, Snap-back induced hysteresis in an elastic mechanical metamaterial under tension, Appl. Phys. Lett. 115 (9) (2019).
[31] S. Wang, J. Guo, A. Biczo, N. Feng, Design and macroscopic mechanical responses of auxetic metamaterials with tunable stiffness, Mater. Des. (2024) 112913.
[32] W. Gao, J. Kang, G. Wang, H. Ma, X. Chen, M. Kadic, V. Laude, H. Tan, Y. Wang, Programmable and variable-stiffness robotic skins for pneumatic actuation, Adv. Intell. Syst. (2023) 2300285.
[33] A. Hasse, K. Mauser, Poisson induced bending actuator for soft robotic systems, Soft Robot. 7 (2) (2020) 155–167.
[34] Q. Pan, S. Chen, F. Chen, X. Zhu, Programmable soft bending actuators with auxetic metamaterials, Sci. China, Technol. Sci. 63 (12) (2020) 2518–2526.
[35] A. Rafsanjani, K. Bertoldi, Buckling-induced Kirigami, Phys. Rev. Lett. 118 (8) (2017) 084301.
[36] A. Rafsanjani, Y. Zhang, B. Liu, S.M. Rubinstein, K. Bertoldi, Kirigami skins make a simple soft actuator crawl, Sci. Robot. 3 (15) (2018) eaar7555.
[37] N. An, A.G. Domel, J. Zhou, A. Rafsanjani, K. Bertoldi, Programmable hierarchical Kirigami, Adv. Funct. Mater. 30 (6) (2020) 1906711.
[38] A. Rafsanjani, L. Jin, B. Deng, K. Bertoldi, Propagation of pop ups in Kirigami shells, Proc. Natl. Acad. Sci. 116 (17) (2019) 8200–8205.
[39] C. Branyan, A. Rafsanjani, K. Bertoldi, R.L. Hatton, Y. Mengüç, Curvilinear Kirigami skins let soft bending actuators slither faster, Front. Robot. AI 9 (2022) 872007.
[40] L. Jin, A.E. Forte, B. Deng, A. Rafsanjani, K. Bertoldi, Kirigami-inspired inflatables with programmable shapes, Adv. Mater. 32 (33) (2020) 2001863.
[41] S. Chen, Y. Wang, D. Li, F. Chen, X. Zhu, Enhancing interaction performance of soft pneumatic-networks grippers by skeleton topology optimization, Sci. China, Technol. Sci. 64 (12) (2021) 2709–2717.
[42] D. Wang, C. Jiang, G. Gu, Modeling and design of lattice-reinforced pneumatic soft robots, IEEE Trans. Robot. (2023).
[43] A circle fitting library for python, https://pypi.org/project/circle-fit/.
[44] G. Mao, T. Li, Z. Zou, S. Qu, M. Shi, Prestretch effect on snap-through instability of short-length tubular elastomeric balloons under inflation, Int. J. Solids Struct. 51 (11–12) (2014) 2109–2115.
[45] J.T. Overvelde, T. Kloek, J.J. D'haen, K. Bertoldi, Amplifying the response of soft actuators by harnessing snap-through instabilities, Proc. Natl. Acad. Sci. 112 (35) (2015) 10863–10868.
[46] Ecoflex 00-30 product information, smooth-on, inc., https://www.smooth-on.com/products/ecoflex-00-30/. (Accessed 16 September 2024).
[47] S. Tang, K. Tang, S. Wu, Y. Xiao, S. Liu, J. Yi, Z. Wang, Performance enhancement of the soft robotic segment for a trunk-like arm, Front. Robot. AI 10 (2023) 1210217.
[48] J. Libby, A.A. Somwanshi, F. Stancati, G. Tyagi, A. Patel, N. Bhatt, J. Rizzo, S.F. Atashzar, What happens when pneu-net soft robotic actuators get fatigued?, in: 2023 International Symposium on Medical Robotics (ISMR), IEEE, 2023, pp. 1–6.
[49] F. Wenz, I. Schmidt, A. Leichner, T. Lichti, S. Baumann, H. Andrae, C. Eberl, Designing shape morphing behavior through local programming of mechanical metamaterials, Adv. Mater. 33 (37) (2021) 2008617.
[50] D. Schwarz, G. Felsch, F. Tauber, S. Schiller, V. Slesarenko, Exploiting self-contact in mechanical metamaterials for new discrete functionalities, Mater. Des. 236 (2023) 112468.
[51] Y.-F. Zhang, C.J.-X. Ng, Z. Chen, W. Zhang, S. Panjwani, K. Kowsari, H.Y. Yang, Q. Ge, Miniature pneumatic actuators for soft robots by high-resolution multimaterial 3d printing, Adv. Mater. Technol. 4 (10) (2019) 1900427.
[52] S. Li, S.A. Awale, K.E. Bacher, T.J. Buchner, C. Della Santina, R.J. Wood, D. Rus, Scaling up soft robotics: a meter-scale, modular, and reconfigurable soft robotic system, Soft Robot. 9 (2) (2022) 324–336.
[53] C. Tawk, G. Alici, A review of 3d-printable soft pneumatic actuators and sensors: research challenges and opportunities, Adv. Intell. Syst. 3 (6) (2021) 2000223.
[54] N. An, Q. Jia, H. Jin, X. Ma, J. Zhou, Multiscale modeling of viscoelastic behavior of unidirectional composite laminates and deployable structures, Mater. Des. 219 (2022) 110754.

Supplementary Information for Robotic skins inspired by auxetic metamaterials for programmable bending of soft actuators

Yichen Pu[1], Shengwei Zheng[1], Xinjie Hu[1], Shan Tang[2], and Ning An[1,2*]

[1]*Key Laboratory of Advanced Spatial Mechanism and Intelligent Spacecraft, Ministry of Education, School of Aeronautics and Astronautics, Sichuan University, Chengdu 610065, People's Republic of China and*

[2]*State Key Laboratory of Structural Analysis for Industrial Equipment, Dalian University of Technology, Dalian 116023, People's Republic of China*

(Dated: September 17, 2024)

*Correspondence to anning@scu.edu.cn (Ning An)

I. GEOMETRY OF UNIT CELL

Fig. S1 provides a detailed representation of the beam thickness of the unit cell for both the negative Poisson ratio (NPR) and positive Poisson ratio (PPR) metamaterials.

II. EXPERIMENT

Fig. S2 illustrate the experimental setup to measure the bending deformation of the pneumatic actuator upon controlled air pumping. The soft actuator was connected to a syringe pump (LSP01-3A, LongerPump, UK) to control the airflow at a low rate of 125 mL/min. A digital pressure gauge (YK-120B, Shelok, China), along with computer code, was employed to monitor the air pressure within the actuators. Besides, a digital camera (SONY α6000) was placed in front of the soft actuator to capture snapshots of the deformation upon air pumping. The coordinates data of the boundary profile of the actuator were extracted using the WebPlotDigitizer software. This tool allows for precise digitization of the actuator's boundary profile from experimental images, enabling accurate curvature fitting for the deformation analysis.

III. MECHANICAL BEHAVIOR OF METAMATERIAL SKINS

To further characterize the mechanical behavior of the metamaterial-inspired robotic skins, we conducted finite element (FE) simulations using the commercially available package ABAQUS/Standard 2020. In all simulations, the models were discretized using three-dimensional quadratic tetrahedral elements with a hybrid formulation (ABAQUS element type: C3D10H). The cylindrical robotic skin was flattened into two dimensions and subjected to uniaxial tension in the vertical and horizontal directions, respectively. The material behavior was captured using a neo-Hookean material model with material properties detailed in the manuscript. The implicit dynamics solver with the quasi-static option in ABAQUS was employed to simulate the deformation process.

Fig. S3 illustrates the mechanical response of the robotic skin for Specimen-I as presented in Fig. 4 in the manuscript. Fig. S3(A) presents the geometry of the robotic skin viewed in planar view. Figs. S3(B) and S3(C) depict the reaction force in the y-direction and displacement in the x-direction of the NPR and PPR metamaterials when subjected to y-

directional displacement. Figs. S3(D) and S3(E) show the reaction force in the x-direction and displacement in the y-direction of the NPR and PPR metamaterials when subjected to x-directional displacement. It can be seen that the NPR metamaterial has a significantly lower tension stiffness than the PPR metamaterial in both x- and y-directions. Additionally, NPR exhibits a pronounced negative Poisson ratio in both directions, whereas PPR exhibits a pronounced positive Poisson ratio in both directions.

Fig. S4 shows the effect of the number of unit cells in the vertical direction, denoted as n_v, on the mechanical response of the robotic skins. In these simulations, the longitudinal length of the metamaterial is fixed as a constant $L = 104.3$ mm, and n_v varies from 5, 7, to 9. Figs. S4(B) and S4(C) illustrate the reaction force in the y-direction and displacement in the x-direction of the NPR and PPR metamaterials when subjected to y-directional displacement. Figs. S4(D) and S4(E) depict the reaction force in the x-direction and displacement in the y-direction of the NPR and PPR metamaterials when subjected to x-directional displacement. It is observed that as n_v increases, both the NPR and PPR materials undergo a reduction in tension stiffness in the longitudinal direction, while experiencing an increase in tension stiffness in the horizontal direction. Furthermore, the NPR metamaterial experiences a significant decrease in the negative Poisson effect in the longitudinal direction, but undergoes an increase in the negative Poisson effect in the horizontal direction.

Fig. S5 shows the effect of the number of unit cells in the horizontal direction, denoted as n_h, on the mechanical response of the robotic skins. In these simulations, the horizontal width of the metamaterial is fixed as a constant of $2\pi R$, where $R = 14.5$ mm represents the cross-sectional radius of the soft tube, and n_h varies from 12, 16, to 20. Figs. S5(B) and S5(C) illustrate the reaction force in the y-direction and displacement in the x-direction of the NPR and PPR metamaterials when subjected to y-directional displacement. Figs. S5(D) and S5(E) depict the reaction force in the x-direction and displacement in the y-direction of the NPR and PPR metamaterials when subjected to x-directional displacement. It is observed that as n_h increases, both the NPR and PPR materials undergo an increase in tension stiffness in the longitudinal direction, while experiencing a reduction in tension stiffness in the horizontal direction. Moreover, the NPR metamaterial experiences an increase in the negative Poisson effect in the longitudinal direction, but undergoes a decrease in the negative Poisson effect in the horizontal direction.

Fig. S6 illustrates the influence of the material modulus on the mechanical response of the robotic skins. The geometric parameters for the metamaterial are consistent with those presented in Table 1 of the manuscript. The initial shear modulus of the robotic skin is set to $\alpha \cdot \mu$, where α is the modulus ratio of the robotic skin to the soft tube, which varies from 20, 50, to 80, and $\mu = 0.037$ MPa represents the initial shear modulus of the soft tube. It is shown that as the modulus of the skin material increases, both the NPR and PPR metamaterials become proportionally stiffer in both the longitudinal and horizontal directions, while the Poisson effect remains almost unchanged.

IV. DESIGN OF SOFT ACTUATORS WITH PROGRAMMABLE BENDING RESPONSE

We now explore the potential for achieving more intricate programmable bending with the metamaterial skins. This section presents several examples demonstrated through our FE simulations. In all these examples, the geometric parameters of the NPR and PPR metamaterial unit cells align with those listed in Table 1 of the manuscript. Only the parameters c_g, n_v, and n_h are adjusted as needed.

Fig.S7 showcases the design of a soft actuator replicating the bending motion of a human finger. This actuator consists of three segments connected in series, each characterized by different c_g values, enabling a variation in bending curvature along its longitudinal direction. Fig.S8 illustrates two soft actuators mimicking the in-plane bending and out-of-plane twisting of an elephant's trunk, achieved through the heterogeneous distribution of NPR and PPR metamaterials. Figs.S9-S11 depict the design of three English characters, "S", "C", and "U", showcasing the shape-morphing capability of the proposed concept. Fig. S12 displays a soft actuator resembling the complex bending of octopus tentacles, achieved through a combination of tuning bending curvature and hoop expansion. The actuator transforms from an initially cylindrical shape to a conical shape with intricate bending upon inflation.

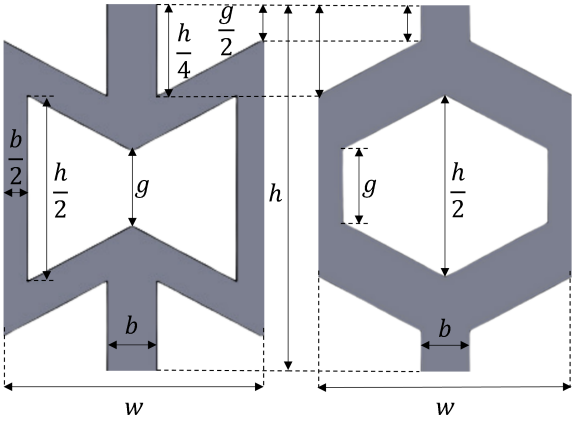

Figure S1: Comprehensive schematic of the unit cell showing the beam thickness. (a) Negative Poisson ratio (NPR) unit cell. (b) Positive Poisson ratio (PPR) unit cell.

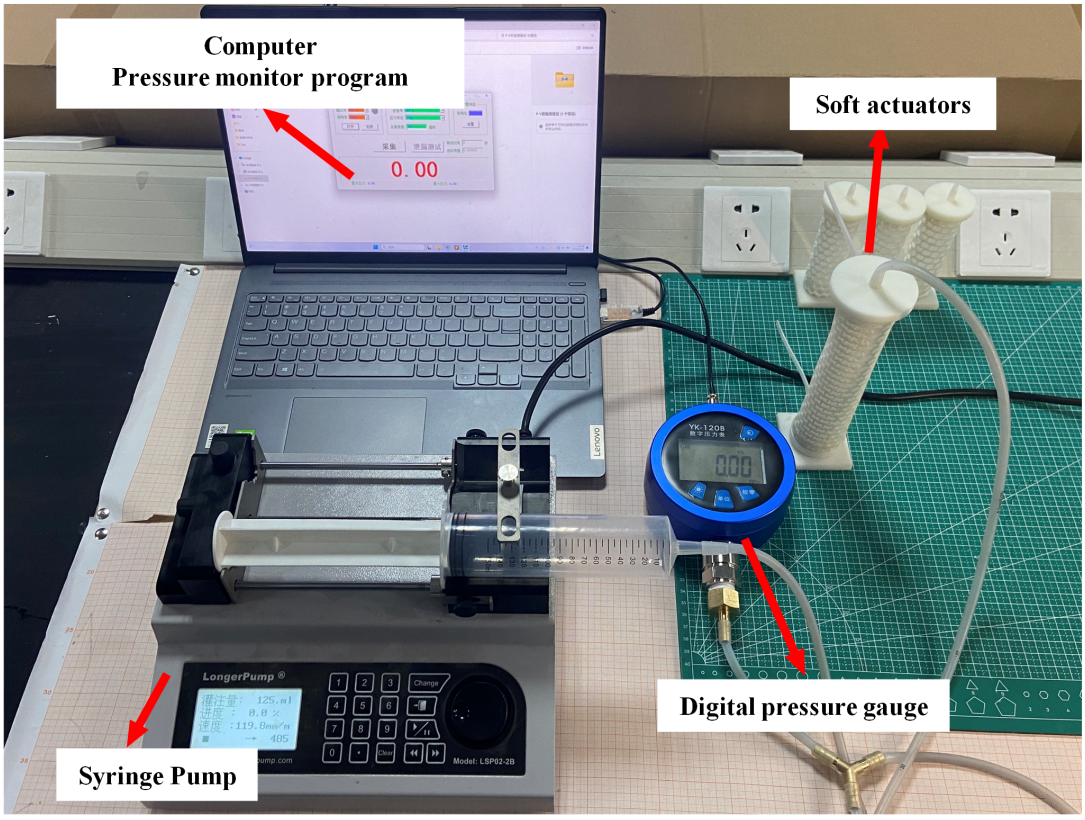

Figure S2: Experimental setup for measuring the deformation of the actuator under controlled inflation volume and pressure. The soft actuator is connected to a digital pressure gauge for precise pressure measurement and a syringe pump for controlled air volume delivery. Besides, a digital camera is used to capture deformation snapshots of the actuator.

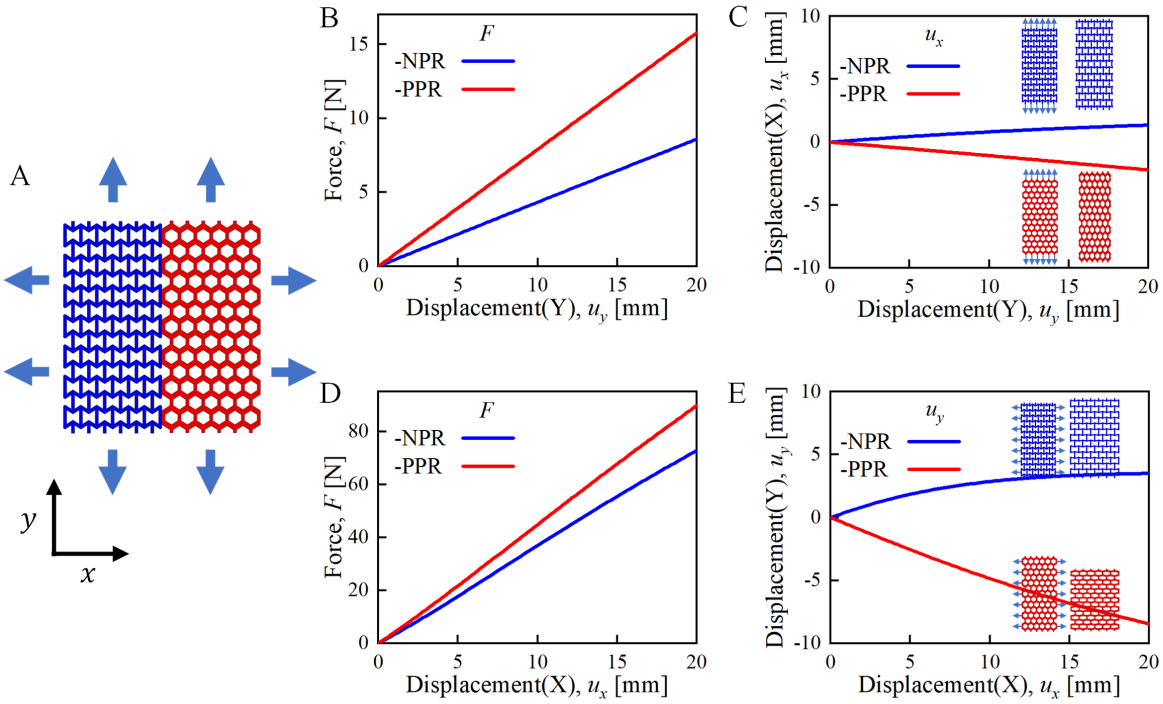

Figure S3: Mechanical response of mechanical metamaterials under uniaxial tension. (A) Robotic skin of Specimen-I viewed in planar orientation. The left NPR and right PPR metamaterials undergo uniaxial tension along the x- and y-directions, respectively. (B) and (C) depict the reaction force in the y-direction and displacement in the x-direction of the NPR and PPR metamaterials when subjected to y-directional displacement. (D) and (E) show the reaction force in the x-direction and displacement in the y-direction of the NPR and PPR metamaterials when subjected to x-directional displacement. In this and the following figures, NPR and PPR metamaterials are represented by blue and red colors, respectively.

V. MOVIE CAPTIONS

Movie S1 Bending response of Specimen-I: experiment vs FE simulation.

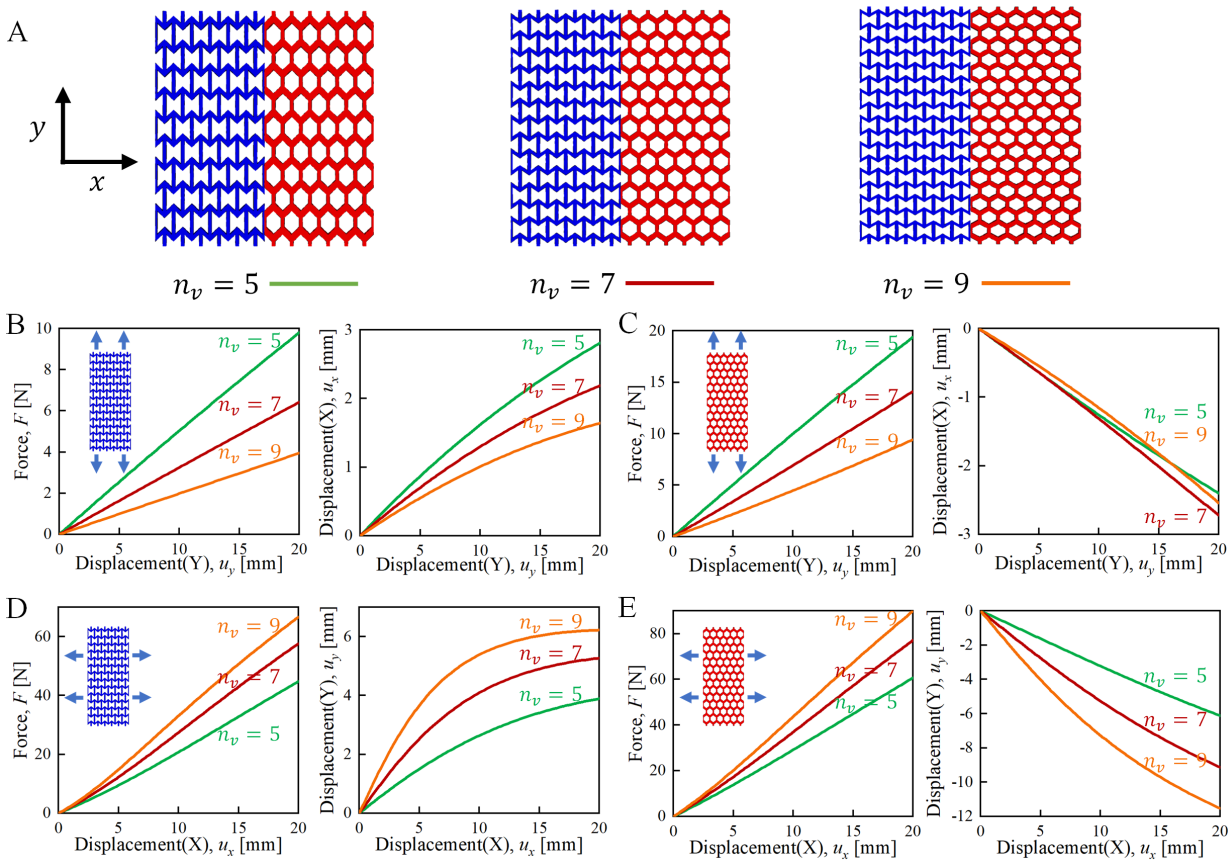

Figure S4: Effect of the number of unit cells in the vertical direction, denoted as n_v, on the mechanical response of the robotic skins. (A) The longitudinal length of the metamaterial is fixed as a constant $L = 104.3$ mm, and n_v varies from 5, 7, to 9. (B) and (C) illustrate the reaction force in the y-direction and displacement in the x-direction of the NPR and PPR metamaterials when subjected to y-directional displacement. (D) and (E) depict the reaction force in the x-direction and displacement in the y-direction of the NPR and PPR metamaterials when subjected to x-directional displacement.

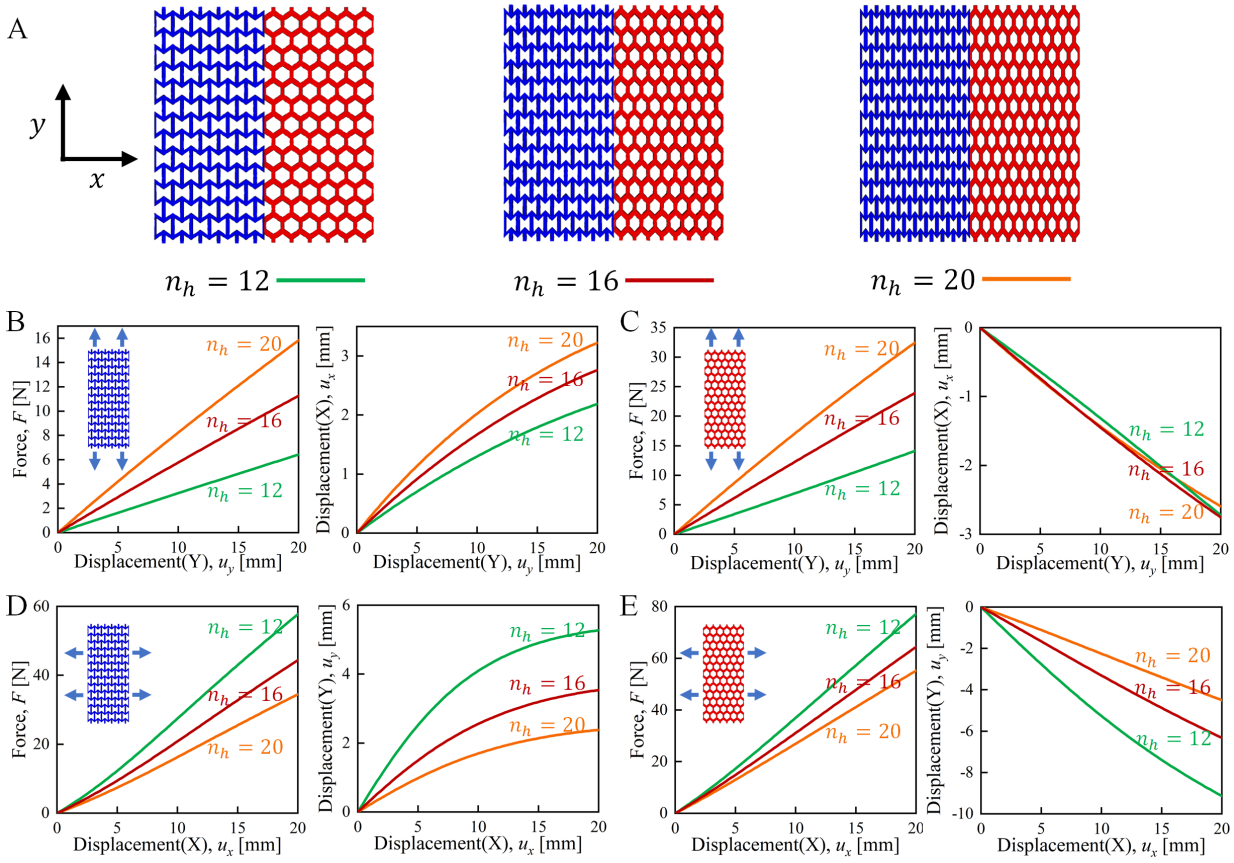

Figure S5: Effect of the number of unit cells in the horizontal direction, denoted as n_h, on the mechanical response of the robotic skins. (A) The horizontal width of the metamaterial is fixed as a constant of $2\pi R$, where $R = 14.5$ mm is the cross-sectional radius of the soft tube, and n_h varies from 12, 16, to 20. (B) and (C) illustrate the reaction force in the y-direction and displacement in the x-direction of the NPR and PPR metamaterials when subjected to y-directional displacement. (D) and (E) depict the reaction force in the x-direction and displacement in the y-direction of the NPR and PPR metamaterials when subjected to x-directional displacement.

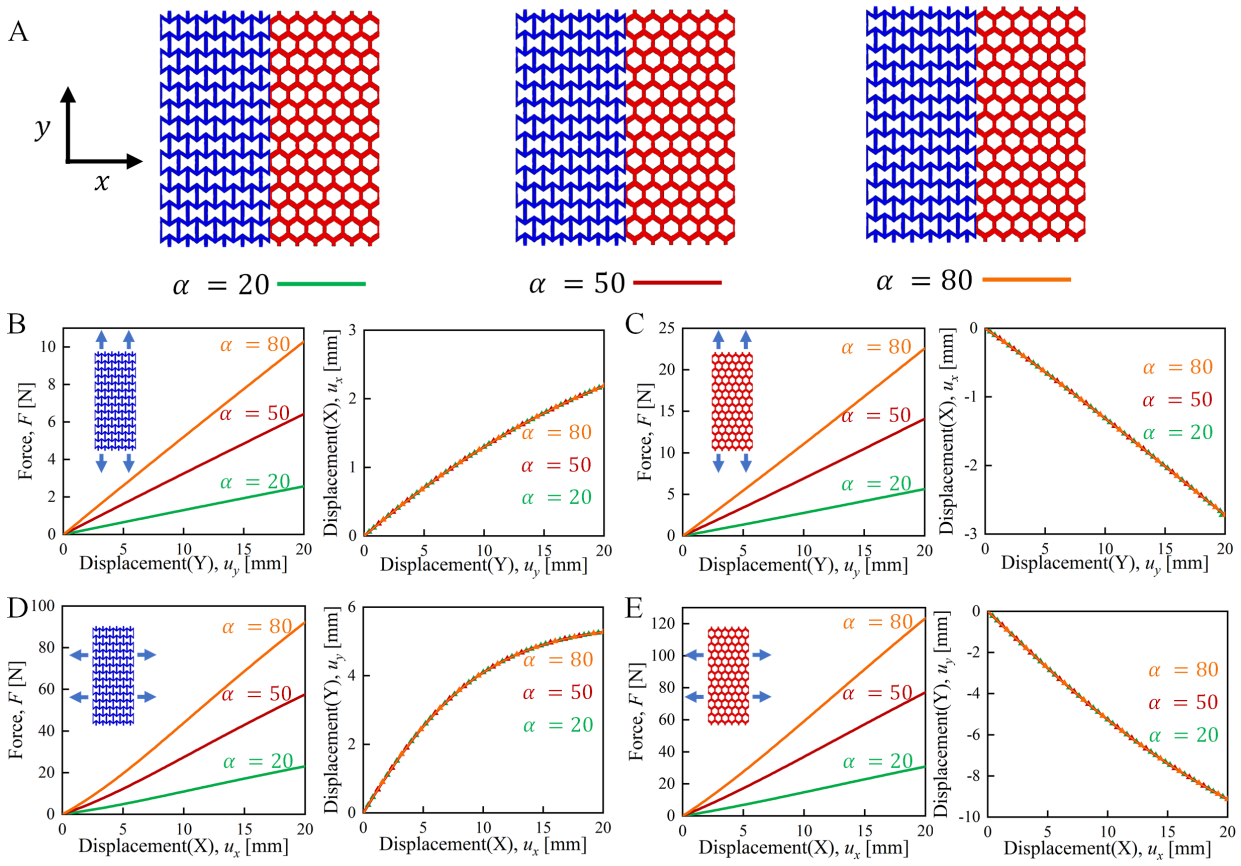

Figure S6: Effect of the initial shear modulus of the material on the mechanical response of the robotic skins. (A) The initial shear modulus of the skin material is set to $\alpha \cdot \mu$, where α is the modulus ratio of the robotic skin to the soft tube, which varies from 20, 50, to 80, and $\mu = 0.037$ MPa represents the initial shear modulus of the soft tube. (B) and (C) illustrate the reaction force in the y-direction and displacement in the x-direction of the NPR and PPR metamaterials when subjected to y-directional displacement. (D) and (E) depict the reaction force in the x-direction and displacement in the y-direction of the NPR and PPR metamaterials when subjected to x-directional displacement.

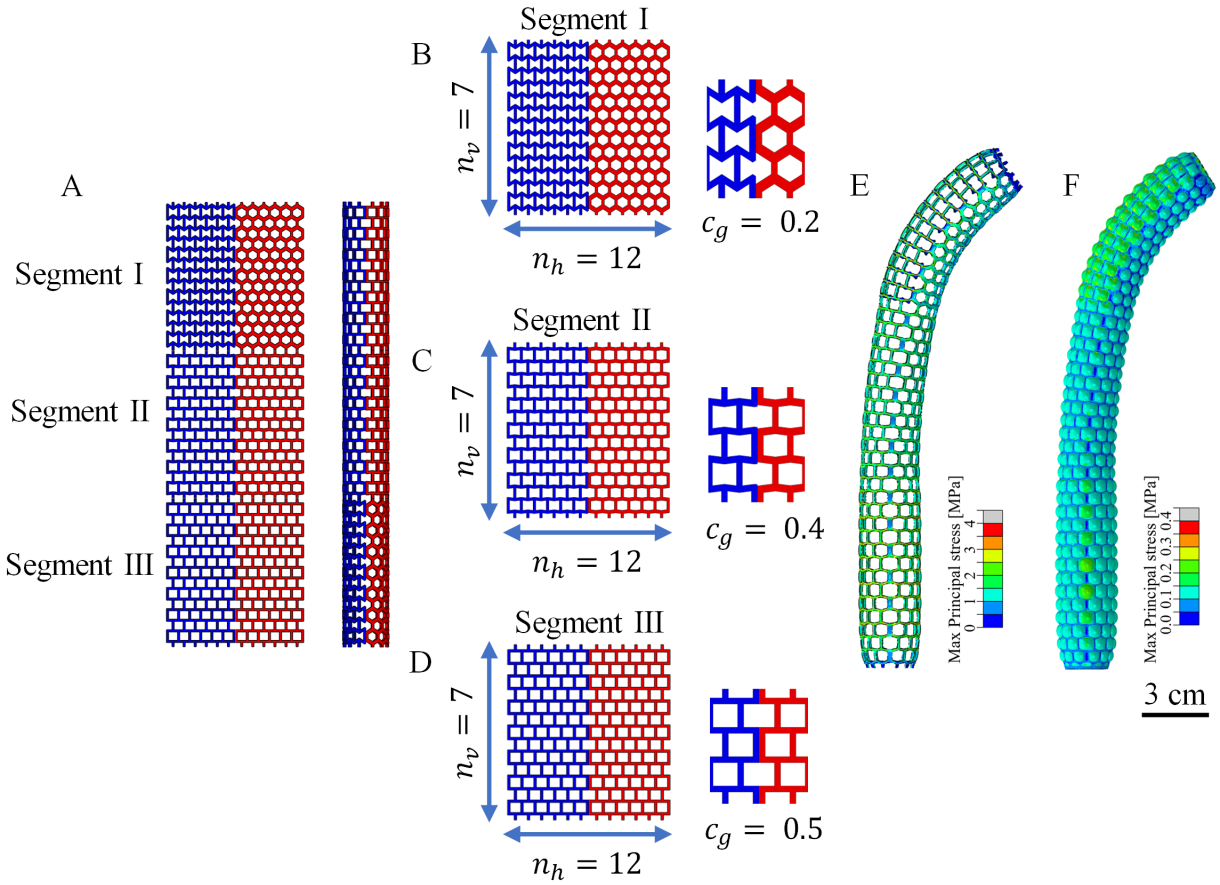

Figure S7: Design of a soft actuator mimicking the bending of a human finger. (A) Schematic of the metamaterial skin in planar view, featuring three segments connected in series. (B)-(D) Segments I, II, and III are characterized by c_g values of 0.2, 0.4, and 0.5, respectively. (E)-(F) The deformation snapshots and stress distributions for both the inflatable tube and the metamaterial skins illustrating bending variations along the longitudinal direction resulting from geometric design variations of the robotic skin. The deformation is achieved by inflating the actuator with an air pressure of 28 kPa.

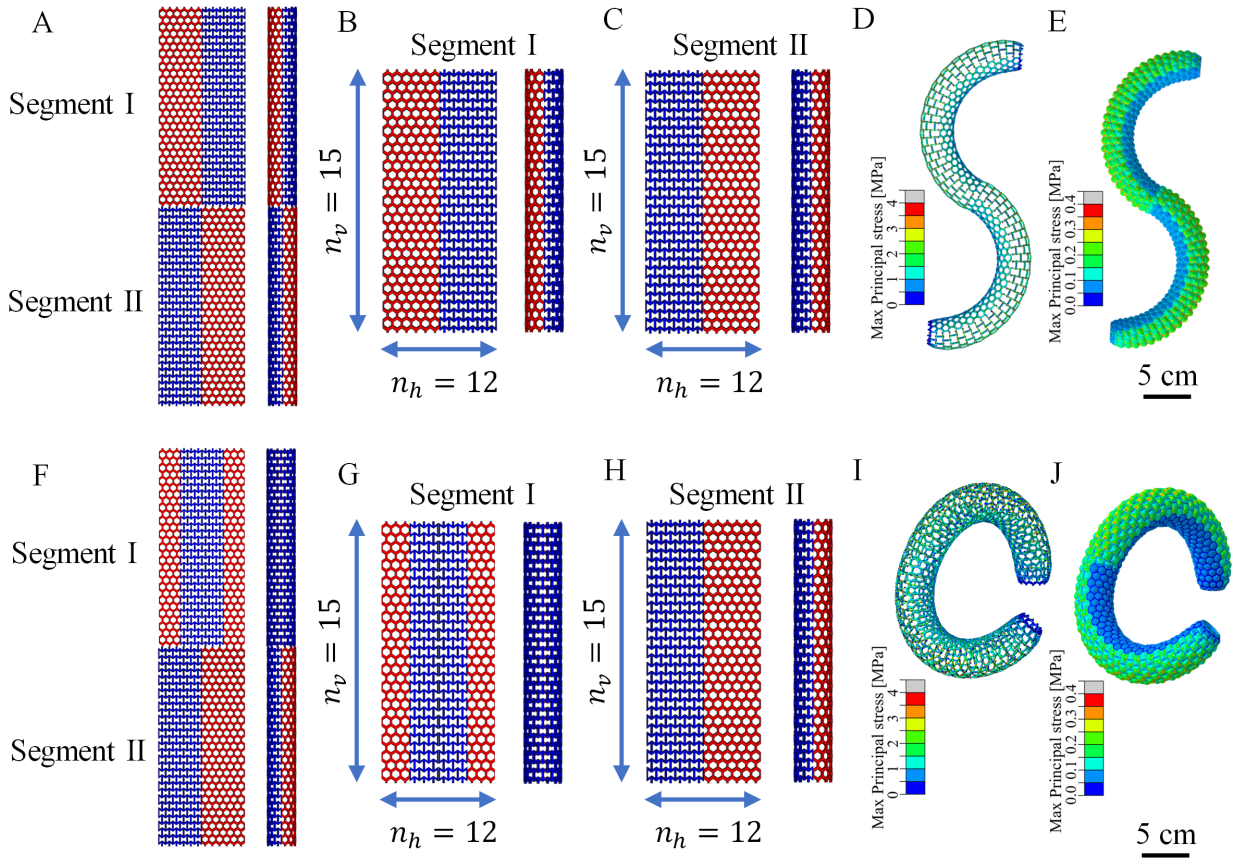

Figure S8: Design of two soft actuators mimicking the in-plane bending and out-of-plane twisting of an elephant's trunk. (A) Planar schematic of the metamaterial skin for the in-plane bending actuator, consisting of two segments connected in series. (B)-(C) Segments I and II feature an inverse arrangement of the NPR and PPR materials. Segment I has NPR on the right and PPR on the left, while Segment II has NPR on the left and PPR on the right. (D)-(E) The deformation snapshots and stress distributions for both the inflatable tube and the metamaterial skins illustrating reverse in-plane bending along the longitudinal direction. The deformation is achieved by inflating the actuator with an air pressure of 28 kPa. (F) Planar schematic of the metamaterial skin for the out-of-plane twisting actuator, also comprising two segments connected in series. (G)-(H) Segments I and II feature a different arrangement of the NPR and PPR materials. Segment I has NPR on the left and PPR on the right, while Segment II has NPR in the middle and PPR on the two sides. (I)-(J) The deformation snapshots and stress distributions for both the inflatable tube and the metamaterial skins illustrating out-of-plane twisting of the actuator. The deformation is achieved by inflating the actuator with an air pressure of 28 kPa.

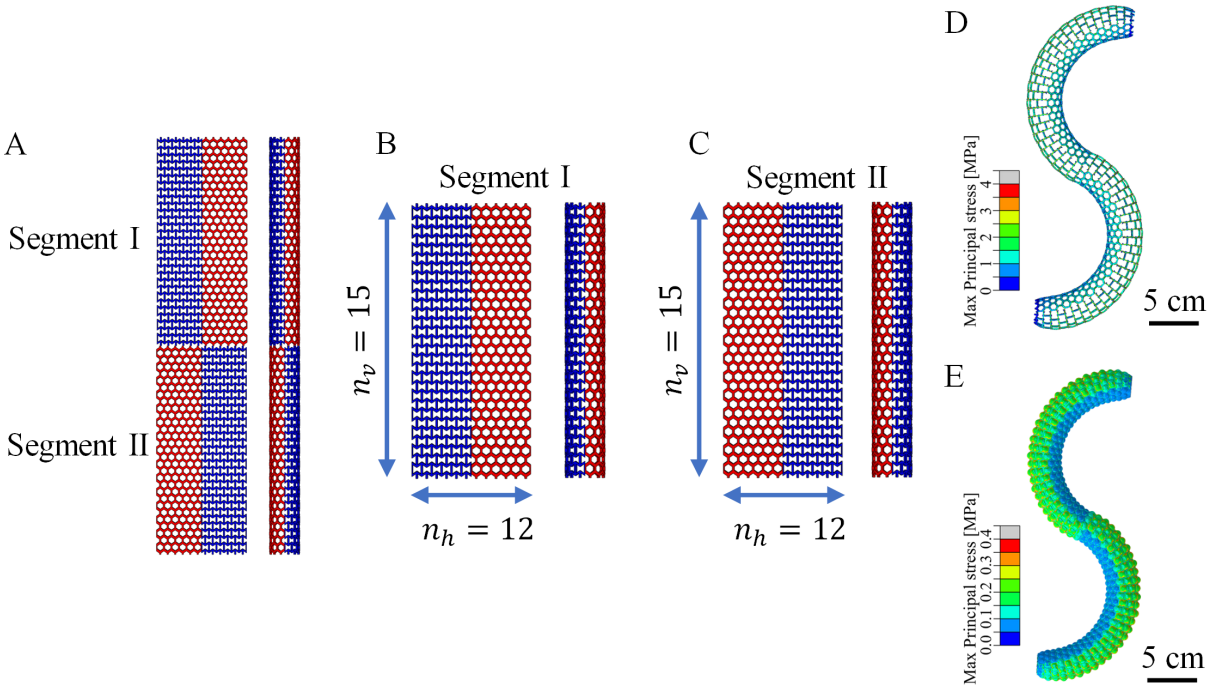

Figure S9: Design of a soft actuator mimicking customized English character "S" shape. (A) Planar schematic of the metamaterial skin for the "S" shape-morphing actuator. It is similar to the in-plane bending of the elephant's trunk. (B)-(C) Segments I and II feature an inverse arrangement of the NPR and PPR materials. Segment I has NPR on the left and PPR on the right, while Segment II has NPR on the right and PPR on the left. (D)-(E) The deformation snapshots and stress distributions for both the inflatable tube and the metamaterial skins illustrating "S" shape under inflation. The deformation is achieved by inflating the actuator with an air pressure of 28 kPa.

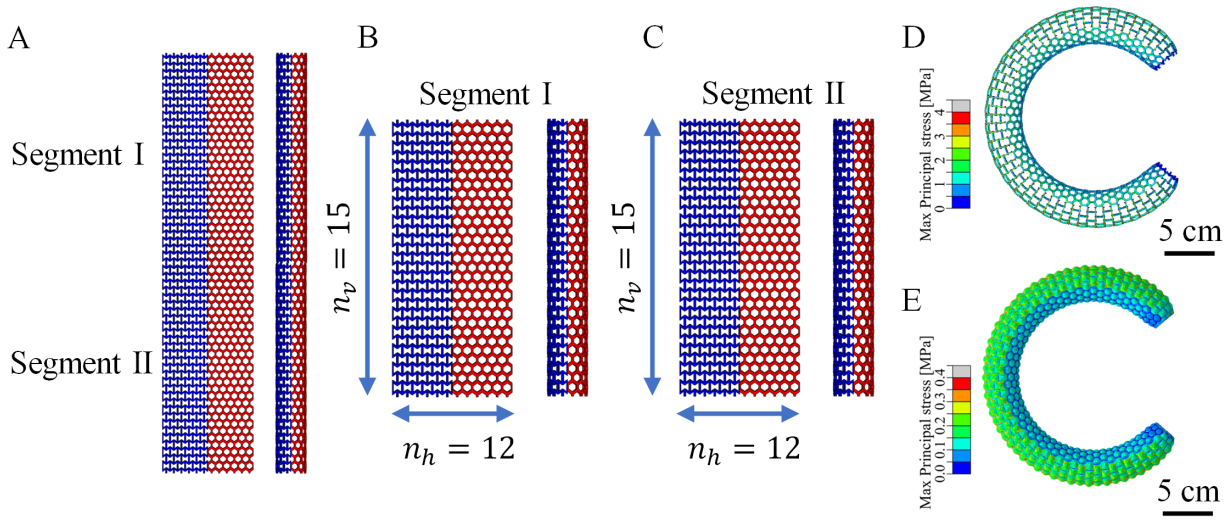

Figure S10: Design of a soft actuator mimicking a customized English character "C" shape. (A) Planar schematic of the metamaterial skin for the "C" shape-morphing actuator, comprising two identical segments connected in series. (B)-(C) Segments I and II feature an identical arrangement of the NPR and PPR materials, with NPR on the left and PPR on the right. (D)-(E) The deformation snapshots and stress distributions for both the inflatable tube and the metamaterial skins illustrating the "C" shape under inflation. The deformation is achieved by inflating the actuator with an air pressure of 28 kPa.

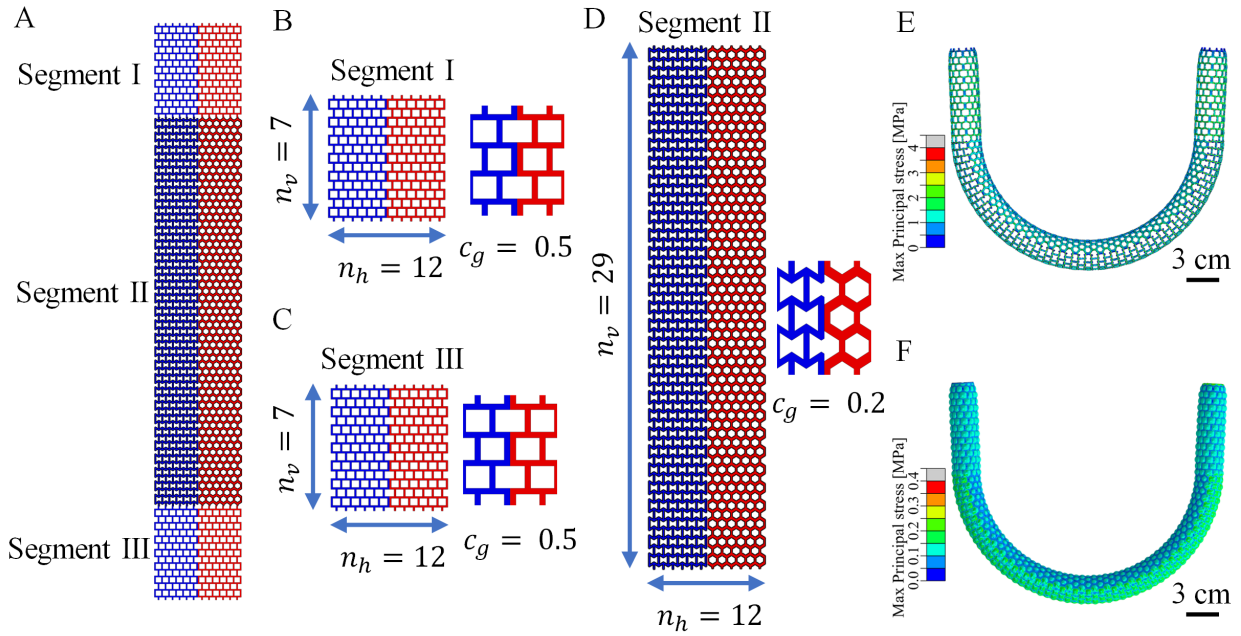

Figure S11: Design of a soft actuator mimicking a customized English character "U" shape. (A) Planar schematic of the metamaterial skin for the "U" shape-morphing actuator, consisting of three segments connected in series. (B)-(D) Segments I and III feature an identical arrangement of the NPR and PPR materials, with NPR on the left and PPR on the right, with $c_g = 0.5$. Segment II features a similar arrangement of the NPR and PPR materials, with $c_g = 0.2$. (E)-(F) The deformation snapshots and stress distributions for both the inflatable tube and the metamaterial skins illustrating the "U" shape under inflation. The deformation is achieved by inflating the actuator with an air pressure of 30 kPa.

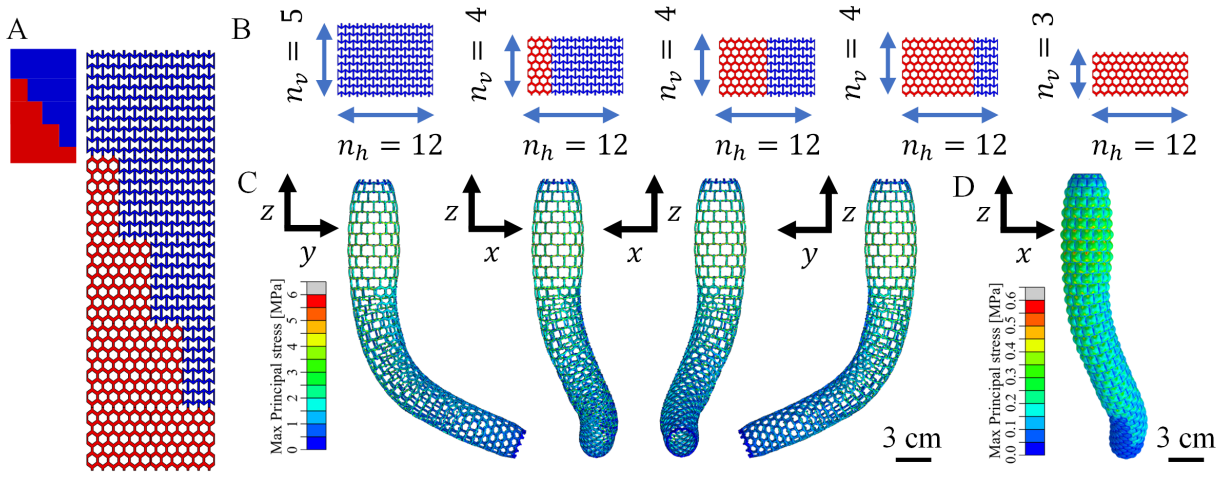

Figure S12: Design of a soft actuator mimicking the complex bending of octopus tentacles. (A) Planar schematic of the metamaterial skin for the octopus tentacle-inspired actuator, consisting of five segments connected in series. (B) Arrangement of the segments from the top to the bottom. (C)-(D) The deformation snapshots and stress distributions for both the inflatable tube and the metamaterial skins illustrating the bending shape of the actuator under inflation. The deformation is achieved by inflating the actuator with an air pressure of 25 kPa.